International
Progress Report

IPR-05-01

Äspö Hard Rock Laboratory

TRUE Block Scale continuation project

BS2B tracer tests with sorbing tracers

Peter Andersson
Johan Byegård
Rune Nordqvist
Eva Wass

GEOSIGMA AB

January 2005

Svensk Kärnbränslehantering AB
Swedish Nuclear Fuel
and Waste Management Co
Box 5864
SE-102 40 Stockholm Sweden
Tel 08-459 84 00
+46 8 459 84 00
Fax 08-661 57 19
+46 8 661 57 19

Äspö Hard Rock
Laboratory

Report no.
IPR-05-01

No.
F56K

Author
Peter Andersson
Johan Byegård
Rune Nordqvist
Eva Wass

Date
Jan. 2005

Checked by
Anders Winberg

Date
2005-05-11

Approved
Anders Sjöland

Date
2005-05-23

Äspö Hard Rock Laboratory

TRUE Block Scale continuation project

BS2B tracer tests with sorbing tracers

Peter Andersson
Johan Byegård
Rune Nordqvist
Eva Wass

GEOSIGMA AB

January 2005

Keywords: TRUE Block Scale, Tracer test, Sorbing, Radioactive, Modelling

Abstract

This report describes the performance and results of tests with radioactive sorbing tracers in the TRUE Block Scale Continuation Project (BS2B). Two tracer injections were performed in different flow paths, one being a flow path within the previously identified Structure #19 and the other being a minor “background fracture” (BG#1) hydraulically connected to Structure #19.

Sammanfattning

Denna rapport behandlar utförandet och resultaten av spårförsök med radioaktiva sorberande ämnen inom TRUE Block Scale Continuation Project (BS2B). Testerna har omfattat två spårförsök i olika flödesvägar. Den ena är en flödesväg inom den tidigare identifierade Struktur #19 och den andra involverar en mindre, singulär, så kallad "bakgrundsspicka" (BG#1) som är hydrauliskt kopplad till Struktur #19.

Executive summary

A programme has been defined to increase the understanding of the processes that govern retention of radionuclides transported in crystalline rock, the Tracer Retention Understanding Experiments (TRUE). The basic idea is to perform a series of tracer tests with progressively increasing complexity.

As a part of the field tracer experiment programme within the TRUE Block Scale Continuation project it was proposed that a tracer experiment with sorbing radioactive tracers should be performed (BS2B). This to facilitate a test of the ability to make predictions of tracer experiments with sorbing tracers on the basis of geological and mineralogical information. Based on the results of the earlier performed experiments, CPT-1 – CPT-4 (Andersson et al, 2004), and the limitation that injections can only be performed in flow paths with a proven recovery >80%, two flow paths of different type were selected for tracer injection.

Specific objectives for the BS2B tracer tests were to study:

- Sorbing tracer transport in a single Type 1 (fault) structure (c.f. Dershowitz et al., 2003) over length scales of tens of metres. The 19.5 m long flow path KI0025F02:R3 → KI0025F03:R3 in Structure #19 was chosen.

- Sorbing tracer transport in a flow path involving a single background fracture of Type 2 (non-fault, c.f Dershowitz et al., 2003) connected to a major Type 1 structure. The only flow path available for tracer experiment addressing this type of transport was the 22 m long flow path KI0025F02:R2 (BG#1, formerly Structure #25) → KI0025F03:R3.

To fulfil the demand of having tracers of different sorption strength, it was considered as advantageous if one sorbing tracer from each group could be used for each flow path. Based on available isotopes, the following selection was done (see also Table 2-1):

- Slightly sorbing tracers: $^{85}Sr^{2+}$ for the fast flow path (KI0025F02: R3 → KI0025F03:R3) and $^{22}Na^{+}$ for the slow flow path (KI0025F02: R2 → KI0025F03:R3).

- Moderately sorbing tracers: $^{86}Rb^{+}$ for the fast flow path and $^{133}Ba^{2+}$ for the slow flow path.

- Strongly sorbing tracers: $^{137}Cs^{+}$ for the fast flow path and $^{54}Mn^{2+}$ for the slow flow path.

The sorbing tracers were also complemented by two non-sorbing tracers in each flow path:

- $^{131}I^{-}$ together with ^{160}Tb-DTPA as tracers for the fast flow path.

- HTO together with ^{155}Eu-DTPA as tracers for the slow flow path.

The tracer tests were performed by establishing a radially converging flow field with a constant withdrawal rate in the selected sink section KI0025F03:R3 (Structure #19). The withdrawal rate was established using the maximum sustainable flow (2.3-2.5 l/min).

Radioactive tracers were injected in the selected injection sections KI0025F02:R2 (BG#1) and KI0025F02:R3 (Structure #19) as decaying pulses with simultaneous injection of water (unlabelled formation water) creating a slight excess pressure and thus, a weak dipole flow field. Samples were automatically withdrawn both in the injection and withdrawal sections and on-line γ-detectors were used.

The BS2B tracer tests were performed using techniques and equipment earlier developed and used in the TRUE Block Scale Phase C experiments (Andersson et al., 2001). In general, the procedures and equipment worked well with only a few minor problems. The only problem that to some degree influences the results is the clogged filter in the circulation loop of KI0025F02:R2, injection section in the slow flow path (BG#1). The resulting poor mixing, especially during the first hours of injection, gives a somewhat uneven tracer distribution. However, the on-line measurement of the input activity makes it possible to take this into account in the evaluation.

The basic preliminary evaluation of the breakthrough data was performed with the same models and concepts as previous tests with sorbing tracers in the TRUE Block Scale, Phase C tests (Andersson et al., 2001). The following main results were obtained:

- Experimental data fits relatively well to a one-dimensional advection-dispersion model with matrix diffusion and linear equilibrium sorption. The fit to the models without matrix diffusion is generally less good.

- The following approximate value ranges for R (retardation coefficient) for the sorbing tracers were found (in rising order):

- $^{85}Sr^{2+}$: 1.1 – 1.25
- $^{22}Na^{+}$: 1.3 – 1.5
- $^{86}Rb^{+}$: 2.9 – 3.2
- $^{133}Ba^{2+}$: 4.1 – 4.5
- $^{54}Mn^{2+}$: 6.4 – 7.4
- $^{137}Cs^{+}$: 12.8 – 13.2

- The values for $^{54}Mn^{2+}$ are associated with large estimation errors. This is also the case, but to a lesser extent, for $^{86}Rb^{+}$.

- The matrix diffusion effect is probably fairly significant in both of the tested flow paths, based on estimated values of parameter A. Further evaluation of A (i.e. to determine D_e) requires estimates of the fracture aperture and the matrix porosity (eq. 4-10). Lower values of A for non-sorbing tracers were found in the faster of the flow paths but, again, the significance of this depends on the values of the aperture and matrix porosity in each flow path.

- Estimated dispersivity values (generally about 2 – 3 m) were in the order of one magnitude smaller than the Euclidian transport distance.

- Estimated residence times were about 10 – 12 hours for the faster flow path, and about 200 – 220 hours for the slower flow path.

- The evaluation of the faster flow path was found to be very sensitive to the injection input function. An accurate description of the injection function was possible by using the on-line measurements at early stages of the injection.

- Theoretical tracer recovery is relatively good for most of the tracers (75-85 %). Significantly lower theoretical recovery was found for three of the sorbing tracers: $^{137}Cs^{+}$ (37 %), $^{133}Ba^{2+}$ (32 %) and $^{54}Mn^{2+}$ (9 %).

The results of the basic modelling show both similarities and differences when compared to the TRUE Block Scale Phase C tests (Andersson et al., 2001). The main difference is that $^{85}Sr^{2+}$ shows a significantly lower retardation than observed in the Phase C tests, in fact also lower than for $^{22}Na^{+}$. The flow paths are also significantly different. Phase C (injection C3) was performed in a long and slow flow path (t_0 =820 h) whereas in this case in a fast flow path (Structure #19, t_0=10 h).

Contents

1 Introduction

1.1 Background

A programme has been defined to increase the understanding of the processes that govern retention of radionuclides transported in crystalline rock, the Tracer Retention Understanding Experiments (TRUE). The basic idea is to perform a series of tracer tests with progressively increasing complexity.

When the TRUE Programme was set up it was identified that the understanding of radionuclide transport and retention in the Block Scale (10-100 m) also required attention in terms of a separate experiment. The TRUE Block Scale project was initiated as an international partnership funded by ANDRA, ENRESA, Nirex, POSIVA, JNC and SKB (Winberg, 1997). The first phase of the TRUE Block Scale Project was finalised during 2002 in the Evaluation and Reporting Stage (Andersson et al., 2002a, b; Poteri et al., 2002; Winberg et al., 2002).

As a part of the field tracer experiment programme within the TRUE Block Scale Continuation project, it was proposed that a tracer experiment with sorbing radioactive tracers should be performed (BS2B). This to facilitate a test of the ability to make predictions of tracer experiments with sorbing tracers on the basis of geological and mineralogical information. Based on the results of the earlier performed experiments, CPT-1 – CPT-4 (Andersson et al., 2004), and the limitation that injections can only be performed in flow paths with a proven recovery >80%, two flow paths of different type were selected for tracer injection.

1.2 Objectives

The overall objective for the tests with radioactive sorbing tracers within the TRUE Block Scale Continuation Project was to increase the understanding of transport and retention of sorbing species in crystalline rock over longer distances (10-100 m).

Specific objectives for the BS2B tracer tests were to study:

- Sorbing tracer transport in a single Type 1 (fault) structure (c.f. Dershowitz et al., 2003) over length scales of tens of metres. The 19.5 m long flow path KI0025F02:R3 → KI0025F03:R3 in Structure #19 was chosen.
- Sorbing tracer transport in a flow path involving a single background fracture of Type 2 (non-fault, c.f Dershowitz et al., 2003) connected to a major Type 1 structure. The only flow path available for tracer experiment addressing this type of transport was the 22 m long flow path KI0025F02:R2 (BG#1, formerly Structure #25) → KI0025F03:R3.

2 Performance and evaluation procedure

2.1 Equipment and tracers used

2.1.1 Borehole equipment

The two characterisation boreholes (KI0025F02 and KI0025F03) involved in the tests are instrumented with 10 inflatable packers each, isolating 9 and 10 borehole sections respectively. The boreholes were re-instrumented before start of the pre-tests (CPT1-4) to better isolate the selected target Structure #19, see Appendix 1. All isolated borehole sections are connected to the HMS-system through data loggers (Datascan). The sections planned to be used for tracer tests are equipped with three nylon hoses, two with an inner diameter of 4 mm and one with an inner diameter of 2 mm. The two 4-mm hoses are used for injection, sampling and circulation in the borehole section whereas the 2-mm hose is used for pressure monitoring.

All materials in contact with the tracer solution have been tested in laboratory tests for the interaction with presumed non-sorbing and cation exchange sorbing tracers (Ittner and Byegård, 1997). The results showed that any sorption was found to be negligible compared to sorption on rock material. Further experiences from earlier performed in-situ tracer studies performed under more realistic field conditions (e.g., TRUE Block Scale Experiment, Andersson et al. 2004) have shown that sorption on borehole equipment is generally a negligible problem. However, at long contact times, a time build-up of some sorbing tracers (e.g., $^{137}Cs^{+}$) on the surfaces of the polyamide lines of the borehole equipment. Furthermore, an immediate pronounced sorption of the strongest sorbing tracers used (i.e., $^{65}Zn^{2+}$ and $^{57}Co^{2+}$) could be observed on the polyamides lines.

2.1.2 Injection equipment

A schematic drawing of the tracer test equipment is shown in Figure 2-1. The equipment is built for establishing an internal circulation in the borehole section. The circulation makes it possible to obtain a homogeneous tracer concentration in the borehole and to sample the tracer concentration outside the borehole in order to monitor the injection rate of the tracer with time.

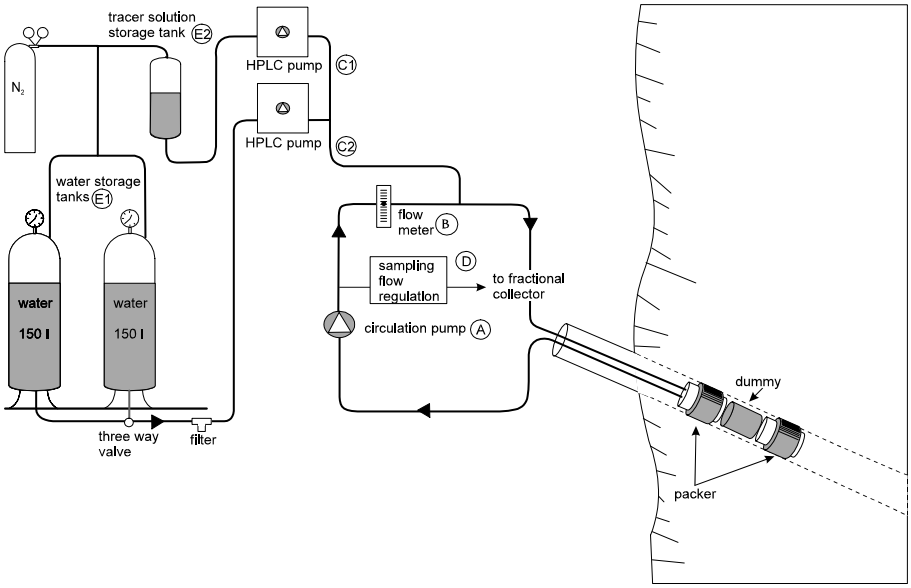

Figure 2-1 *Schematic drawing of the tracer injection/sampling system used in the TRUE Block Scale Continuation Project.*

A pump with a variable speed controller (A) enables and controls circulation rates. The rates are measured by a flow meter (B). In sections with low flow rates, the tracer is forced into the flow path by applying a slight excess pressure using an external water injection pump (providing a weak dipole flow geometry). Water and tracer injections are made with two different HPLC plunger pumps (C1 and C2). Water for injection is stored in a pressurised vessel (E1) under nitrogen atmosphere. The radioactive tracer solution is injected from a 1-litre plastic bottle placed behind lead shields to protect from radiation during the injection procedure. An optional tracer storage vessel is also available (E2) but was not used in these injections.

The tracer concentration (activity) in the injection loop is measured both *in situ* and by sampling and subsequent analyses. The sampling is made by continuously extracting a small volume of water from the system through a flow controller (constant leak) to a fractional sampler (D). The in situ monitoring of tracer content in the injection system is made by using a HpGe-detector measuring on-line on the tubing (γ-emitting radionuclides). The tracer test equipment has earlier been used in the TRUE Block Scale tracer tests (e.g. Andersson et al., 2002b). A thorough description of the equipment and procedures for measurements of the tracer activities/concentrations are given in Section 2.2.

2.1.3 Sampling and detection equipment

The tracer concentration (activity) in the withdrawal water is measured in a similar way as the injection concentrations, i.e. both in situ and by sampling and subsequent analyses. The sampling is made with a 24-valve sampling unit taking discrete 1 litre samples (sampling intervals between 5 minutes up to 100 hours). The in-situ monitoring is handled by a HpGe-detector in order to continuously analyse the breakthrough of γ-emitting radionuclides, see also Section 2.2.

2.1.4 Selection of tracers

Rationale

For the study of the impact of sorption interaction on transport, comparison of the breakthrough of simultaneously injected non-sorbing and sorbing tracers are essential. Furthermore, experiences of earlier sorbing tracer experiments in the TRUE-program, have shown that the use of a cocktail of tracers with different degree of sorption strength has been a quite successful concept.

Regarding the sorbing tracers, the same prerequisites as in the earlier TRUE experiments were considered, i.e.:

- Preferentially, elements from the alkali and alkaline earth metal were selected. These elements are considered to interact with the non-mobile phases by a cation exchange mechanism, which is expected to be fast and reversible.
- To avoid non-linear sorption caused by varying chemical concentrations, radioactive tracers were used. Due to the high specific activity of radioactive tracer, these tracers could provide a dynamic range (i.e., injected activity divided by the detection limit activity) only causing a negligible increase of the chemical concentration.
- Radionuclides with its decay associated with γ-radiation were preferred since γ-spectrometry is the most convenient method for measuring and quantify the concentration of radioactive tracers.

Since radioactive tracers were demanded from the reasons mentioned above, it was due to measurement reasons also decided to also use radioactive non-sorbing tracers.

Two different cocktails with radioactive tracers were to be used in the TRUE Block Scale Continuation Tests with sorbing tracers; one for the faster of the two flow paths selected (KI0025F02:R3 → KI0025F03:R3) and one for the slower flow path (KI0025F02:R2 → KI0025F03:R3), c.f. Table 2-1. The tracers are described in the following sections.

Non-sorbing tracers

The radioactive tracers with its decay associated with γ-radiation that has been used in the TRUE-program so far are $^{82}Br^-$ ($t_{½}$=1.47d), $^{131}I^-$ ($t_{½}$=8.02d) and $^{186}ReO_4^-$ ($t_{½}$=3.72d). All of these tracers are rather short-lived and are therefore, in most tracers tests, not well-suited for studies of the characteristics of the late time arrival ("tailing"). Tritium-labelled water, HTO ($t_{½}$=12.3y), is more long-lived non-sorbing tracers that has been frequently used in the TRUE experiments. However, it has the disadvantage of having a decay that shows no detectable γ-radiation which makes the measurement procedures more complicated, e.g., it can not be measured in the on-line measurements.

As been investigated by Byegård et al. (2000), the use of metal ion complex (e.g., EDTA and DTPA complexes) offers a great potential and flexibility in half-lives in the choice of radioactive non-sorbing tracers. DTPA complexes of lanthanide ions have with good results been used as tracers in the TRUE program (e.g., Andersson, 1996, Holmqvist et al., 2002 and Andersson et al., 2000), however in their non-radioactive

form which demands the use of rather high start concentration (typically in the range of 10 000 ppm). Such high concentrations of complexing agents are obviously not a good choice of non-sorbing tracers in experiments with sorbing tracers; non-metal attached complexing agents may react with the sorbing cations and increase the mobility of these cations. However, the use of complexed radioisotopes allows a significant lower concentration of complexing agent which is not likely to cause this problem.

Limitation of the long term stability of the metal complexes could also be a problem for the use of them as tracers. Based on experiences from laboratory and field investigations (Byegård et al., 2000), elements in the middle of the lanthanide series complexed with DTPA are indicated to be the best choice of tracers among metal complexes. However, since no experiences exist of low concentration use of these tracers, it can not be recommended to use these tracers as the only non-sorbing from one flow path.

Based on the consideration described above, the choice of non-sorbing tracers in this experiment became:

- $^{131}I^-$ together with ^{160}Tb-DTPA as tracers for the fast flow path i.e., KI0025F02:R3 → KI0025F03:R3.
- HTO together with ^{155}Eu-DTPA as tracers for the slow flow path i.e., KI0025F02:R2 → KI0025F03:R3.

Sorbing tracers

Based on laboratory experiments (e.g., Byegård et al., 1998) and earlier experiences from in-situ experiments with sorbing tracers in high saline groundwater (e.g., Winberg et al., 2000, Andersson et al., 2002b) the cation exchange sorbing tracers can be empirically be divided into different groups regarding their general retention properties:

- Slightly sorbing tracers. Only a very minor retardation compared to the non-sorbing tracers. Examples: Na^+ , Ca^{2+} and Sr^{2+}
- Moderately sorbing tracers. Examples: Rb^+ and Ba^{2+}
- Strongly sorbing tracers. Example: Cs^+

Furthermore, the results from the TRUE Block Scale C4 injection (Byegård, 2002) showed high recovery of the tracer $^{54}Mn^{2+}$. This tracer is far much more influenced by hydrolysis than the other tracers mentioned, and is therefore suspected to be a subject for surface complexation. The results of the use this tracer showed that the sorption strength of this tracer should be somewhere between Rb^+ and Cs^+.

A complementary laboratory program has been conducted (Byegård et al, in prep.) where the sorption of these tracers on TRUE Block Scale specific material and non-specific fault gouge material has been studied. The tracers above were included in this study, i.e., cation exchange sorbing tracers and also Mn^{2+}.

To fulfil the demand of having tracers of different sorption strength, it was considered as advantageous if one sorbing tracer from each group could be used for each flow path. Based on available isotopes, the following selection was done (see also Table 2-1):

- Slightly sorbing tracers: $^{85}Sr^{2+}$ for the fast flow path (KI0025F02:R3 → KI0025F03:R3) and $^{22}Na^{+}$ for the slow flow path (KI0025F02:R2 → KI0025F03:R3).
- Moderately sorbing tracers: $^{86}Rb^{+}$ for the fast flow path and $^{133}Ba^{2+}$ for the slow flow path.
- Strongly sorbing tracers: $^{137}Cs^{+}$ for the fast flow path and $^{54}Mn^{2+}$ for the slow flow path.

The isotope selection was made in order to assure a sufficient long half-life to allow studies of the late time arrival (tailing) of the tracers. Unfortunately, at the time for the experiment the isotope $^{83}Rb^{+}$ ($t_{½}$=86.2 d) which was used during the earlier TRUE Block Scale Experiment (Andersson et al., 2002b) was not available from the only known deliver, ORNL Isotope service. Therefore, the more short-lived $^{86}Rb^{+}$ ($t_{½}$=18.7 d) had to be used.

Table 2-1. Tracers used during the TRUE Block Scale Continuation Tests with sorbing tracers. For further details see table 3-2.

Tracer Class	Fast flow path (F02:R3 → F03:R3)	Slow flow path (F02:R2 → F03:R3)
Non-sorbing	$^{131}I^{-}$	HTO
Non-sorbing metal complex	^{160}Tb-DTPA	^{155}Eu-DTPA
Weakly sorbing	$^{85}Sr^{2+}$	$^{22}Na^{+}$
Moderately sorbing	$^{86}Rb^{+}$	$^{133}Ba^{2+}$
Strongly sorbing	$^{137}Cs^{+}$	$^{54}Mn^{2+}$

All radionuclides, except HTO, were analysed by γ-spectrometry. HTO was analysed by liquid scintillation. The measurement procedure is further discussed in Section 2.2.

2.2 Measurements

2.2.1 γ-spectrometry

Samples

Both the samples taken from the injection side and the samples taken from the pump side were diluted to exactly 1000 g and were measured using a 1 litre Marinelli beaker geometry. In order to preserve the samples and to avoid sorption on the beaker walls, 1 ml 65 % nitric acid was added to the solution. All samples were measured using a HpGe detector (35 % relative efficiency, EG&G Ortec) with an automatic sample exchanger (EG&G Ortec). Calibration of the detector was performed using a mixed radionuclide standard (Amersham QCY B41) measured in the same 1 litre Marinelli geometry as the samples.

On-line measurements at injection side

On-line measurements of γ-emitting radionuclides were made on the injection side using a HpGe detector (25 % relative efficiency, Ortec) with a 10 cm thick lead shielding. The measurement cell (see Figure 2-2) consisted of a holder with two nylon tubes (~1 ml) placed at a distance of ~2 cm from the detector. These nylon tubes were thus to be used as parts of the loop used for circulation of the two injection sections. The injection section water was thereby passed by the HPGe-detector and was measured for its concentration of radionuclides with decay associated with γ-radiation.

Before the measurement cell was connected to the circulation loop, each position was calibrated. This was done by a syringe injection of a radionuclide standard solution (Amersham QCY B41) in one of the tubes in the measurement cell. A calibration spectrum was taken up where after the solution was removed from the tube. Before connecting the measurement cell to the circulation line, in order to remove any calibration solution let in the tube, the tube was thoroughly washed with diluted acid and distilled water.

After the first position in the measurement cell had been calibrated, the same procedure was repeated for the second position.

On-line measurements at pump side

For the pump side, an on-line cell was used where all the pumped volume of groundwater could pass by the detector. The online cell, cf. Figure 2-3, consisted of ~140 m of 6/8 mm nylon tubing lined up on a bobbin, yielding a total volume of the flow cell of ~4 litre. The bobbin was placed on an HpGe-detector (18 % relative efficiency, Ortec) and a 4 cm thick lead shielding was placed around the measuring cell. A schematic drawing of the flow cell is given in Figure 2-3.

In order to prevent sorption of radioisotopes in the tubing of the flow cell, a small flow (~0.2 ml/min) of 65 % nitric acid was continuously injected in the water just before its passing through the detector at the pump side.

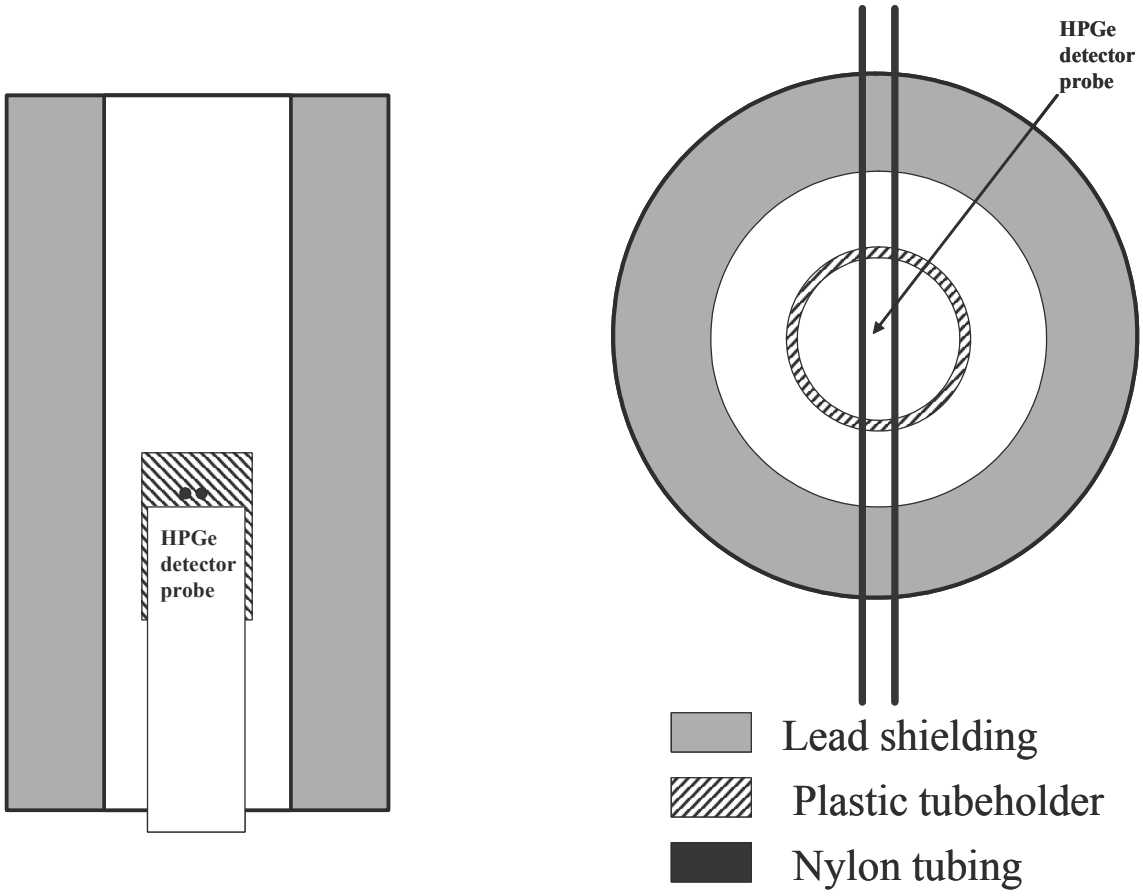

Figure 2-2. *Schematic drawing of the on-line measurement cell used for the injection side, seen from above (left) and from the side (right).*

Due to an early temporarily detector failure and problems with the acid injections, there were large gaps in the data for the on-line measurements on the pump-side. This together with the general disadvantages of on-line measurements compared to sample measurements on the pump side (e.g., lower counting efficiency, more pronounced interferences from the natural concentrations of radon, c.f. Andersson et al. 2001) made quantification using on-line data unnecessary. No calibration procedure (as described in Andersson et al. 2001) was therefore performed for pump side on-line detector in this experiment. Nevertheless, although not used for quantification purposes, on-line measurements were useful for the supervision of the qualitative results of the experiment (e.g., for the observation of breakthrough for the different tracers).

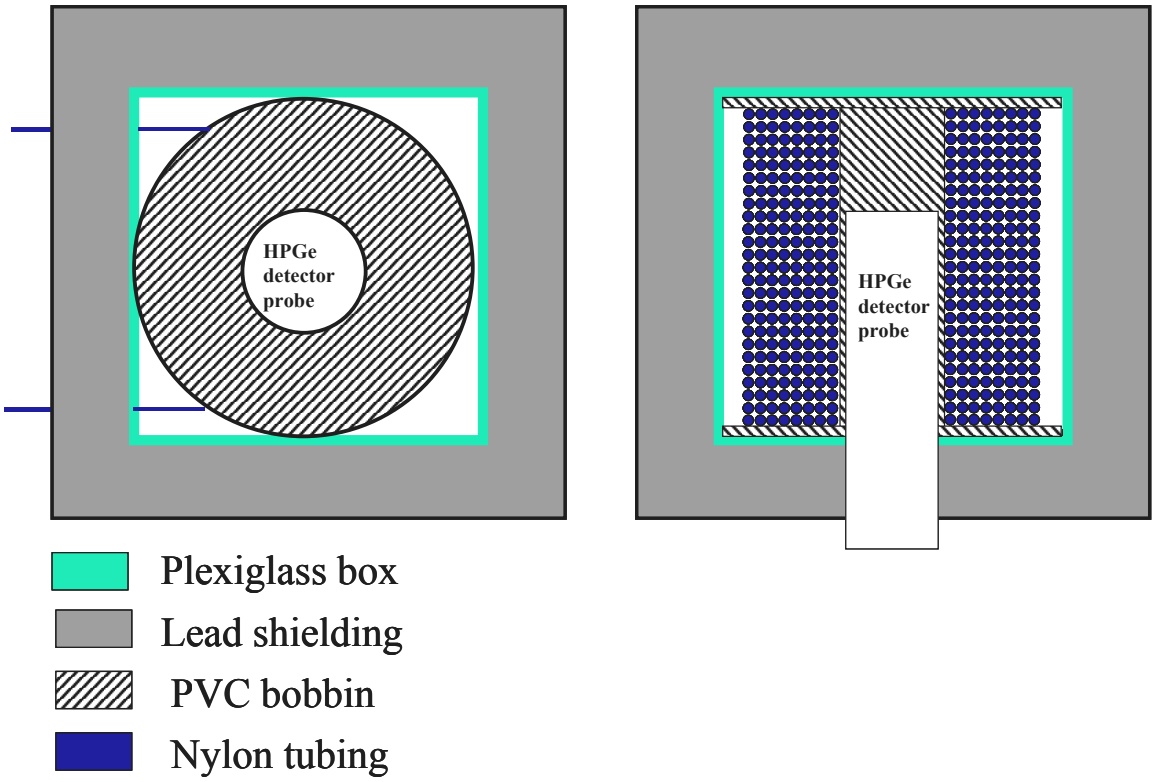

Figure 2-3. *Schematic drawing of the on-line measurement cell used for the pumping side, seen from above (left) and from the side (right).*

Evaluation of γ-spectra

All γ-spectra measured were evaluated using the evaluation procedure in GammaVision ver 5.31 (Ortec). All activities were calculated using a decay correction to the time of the first injection performed (2004-03-31 15.00 in KI0025F02:R3).

2.2.2 Liquid scintillation

The tritiated water tracer (HTO) decays without emission of any measurable γ-energies. Instead of γ-spectrometry, liquid scintillation measurements therefore had to be applied for the quantification of the HTO activity in the samples.

Prior to the measurement, 3 ml of water sample was mixed with 15 ml of scintillation cocktail (Emulsifier Safe, Perkin Elmer). The samples were measured using a liquid scintillation counter Wallac 1414 Guardian. The efficiency calibration was performed using a HTO standard solution (Amersham TRY44).

Contrary to γ-spectrometry, liquid scintillation counting is a qualitatively rather non-specific detection technique. The possibilities to identify what isotopes the different counts originate from are therefore limited. The radioisotopes used simultaneously with HTO are therefore subject for interferences in the liquid scintillation counting of the HTO tracer. In the different TRUE radioactive tracer experiment program, this problem has usually been dealt with by a combination of:

1. Setting the energy discrimination of the measurements so that only β-pulses in the low energy part of the spectrum is registered, i.e., the part of the spectrum where the pulses of the low energetic β-decay of HTO is found.

2. Using a total activity of HTO that is significantly higher than the other radionuclides used simultaneously. This makes the amount of pulses from interfering isotopes negligible compared to the much higher amount of pulses originating from HTO.

However, some remarks have to be made on the consideration of interferences in the HTO measurements in this particular experiment:

For the injection side, it can be seen that the total activity of HTO used is >10 times higher then for the simultaneously injected tracers. Since no significant deviation of the dilution lines could be observed for the sorbing tracers used, there is a strong indication that interferences from the sorbing tracers could be regarded as a minor problem. For this reason, no compensation for interferences from the simultaneously tracers (as described in Andersson et al. 2001) used were used for the measurement of the injection samples. This means that all pulses registered in low energy part of the spectrum were assumed to originate from the decay of HTO, i.e., a minor source for an overestimation of the HTO concentration.

For the pump side, there were occasions when the activity of HTO was expected to be low compared to other tracers present in the water samples. Without any addressing of interferences, it was assumed that a significant overestimation of the HTO activity would be obtained. For this reason, batch-wise ion exchange separation technique was developed, consisting of a:

- 5 ml (exact amount obtained by weighing) groundwater was sampled to a 20 ml scintillation vial.

- 1.5-2 g (exact amount obtained by weighing) of wet and reconditioned mixture of cation and anion exchanger (~50% Dowex 50x4-50 and ~50% Amberlite Cl 50) were added to the vial.

- Samples were thoroughly shaken and were left to stand overnight. The day after, ~3 ml of the water were extracted and passed through a 0.45µm filter and into a new 20 ml scintillation vial. The exact amount of water in the vial was obtained by weighing. This water was than mixed with 15 ml scintillation cocktail and measured as described above.

Evaluation of the HTO concentration in these measurements had to include a compensation for the water content of the ion exchanger; this was determined by an isotope exchange analysis.

The results of the measurement are given in Figure 2.1 where a comparison is made of the results using and not using ion exchange separation. As can be seen, the concentration obtained using the separation is generally slightly lower than the corresponding measurements without ion exchange separation. An interesting observation is the difference of the curves in the first part of the "breakthrough curve". The first peak in the curve representing the non-processed samples actually corresponds to the breakthrough of the non- and weakly sorbing tracers of the injection in KI0025F02:R3, i.e., an injection where HTO was not present. This observation is thus a clear indication of the suitability of the ion exchange process to obtain more correct results for HTO in this type of multi-tracer experiments. For this reason, only the results from the ion change process were used for the representation of the results from the pump side.

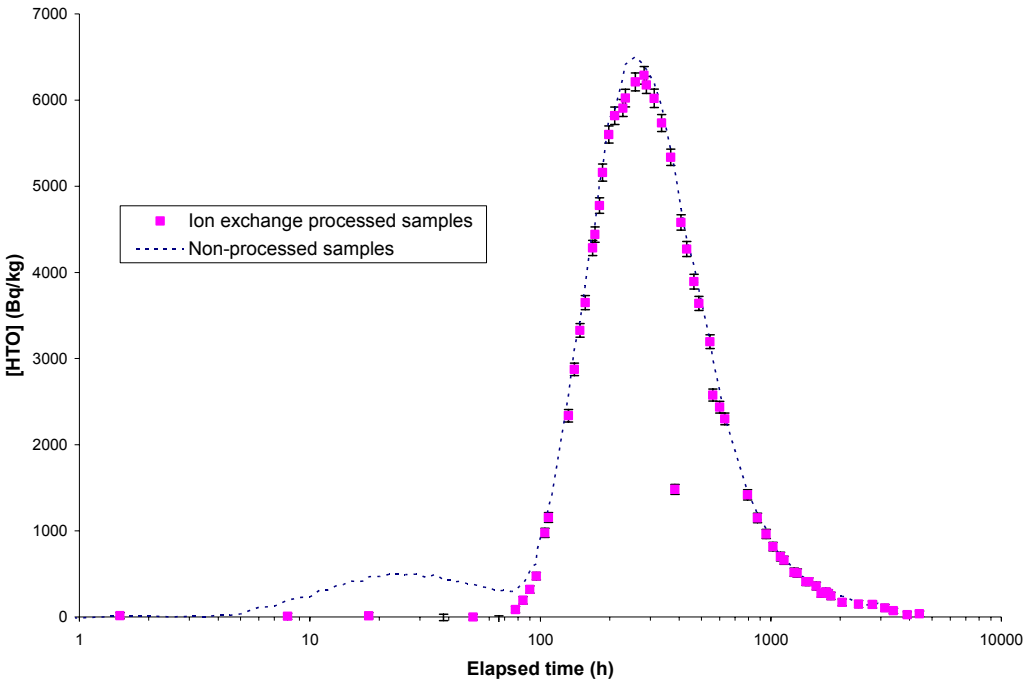

Figure 2-4 *Comparisons of the breakthrough curve of HTO obtained from the ion exchange process (dots) and from the non-processed samples (dashed line)*

The efficiency of the separation process was roughly estimated by spiking a small amount of the different tracers to 5 ml groundwater and processing this solution with the ion exchange method. The γ-activities of the ion exchanger and the extracted solution were measured and the separation efficiency was estimated. The results are given in Table 2-2.

Table 2-2. Separation efficiency for the ion exchange separation of the different ionic tracers used in the experiment

Tracer Class	Fast flow path (F02:R3 – F03:R3)	Separation Efficiency (%)	Slow flow path (F02:R2 – F03:R3)	Separation Efficiency (%)
Non-sorbing	$^{131}I^-$	(decayed)[1]		
Non-sorbing metal complex	^{160}Tb-DTPA	>87	^{155}Eu-DTPA	>81
Weakly sorbing	$^{85}Sr^{2+}$	>89	$^{22}Na^+$	78
Moderately sorbing	$^{86}Rb^+$	(decayed)[1]	$^{133}Ba^{2+}$	>96
Strongly sorbing	$^{137}Cs^+$	85	$^{54}Mn^{2+}$	98

1) $^{131}I^-$ and $^{86}Rb^+$ had decayed at the time when HTO measurement was performed (2004-08-18) which excluded them from this investigation.

2.3 Performance of the radioactive sorbing tracers tests

The TRUE Block Scale Continuation tests BS2B with radioactive sorbing tracers were performed by establishing a radially converging flow field with a constant withdrawal rate in the selected sink section KI0025F03:R3 (Structure #19). The withdrawal rate was established using the maximum sustainable flow (2.3-2.5 l/min).

Radioactive tracers were injected in the selected injection sections KI0025F02:R2 (BG#1) and KI0025F02:R3 (Structure #19) as decaying pulses with simultaneous injection of water (unlabelled formation water) creating a slight excess pressure and thus, a weak dipole flow field. The injection data are presented in Section 3.1.1.

Samples were automatically withdrawn both in the injection and withdrawal sections using techniques and equipment described in Sections 2.1 and 2.2. The resulting tracer breakthrough data are presented in Section 3.1.2.

Two different sets of tracers were used, one for the faster of the two flow paths and one for the slower, cf. Sections 2.1.4 and 3.1.1. Additional parameters monitored were (c.f, Section 3.1.3):

- pressure and hydraulic head (Äspö Hydro Monitoring System)
- withdrawal rate (manual measurements)

Locations of the boreholes and involved borehole sections in the TRUE Block Scale array are shown in Figure 2-5 together with the main interpreted deterministic structures in the investigated rock volume, including Structure #19.

The distances between injection sections and pumping sections employed in the BS2B tests with sorbing tracers, and the CPT-1 through CPT-4 tests, are given in Appendix 2.

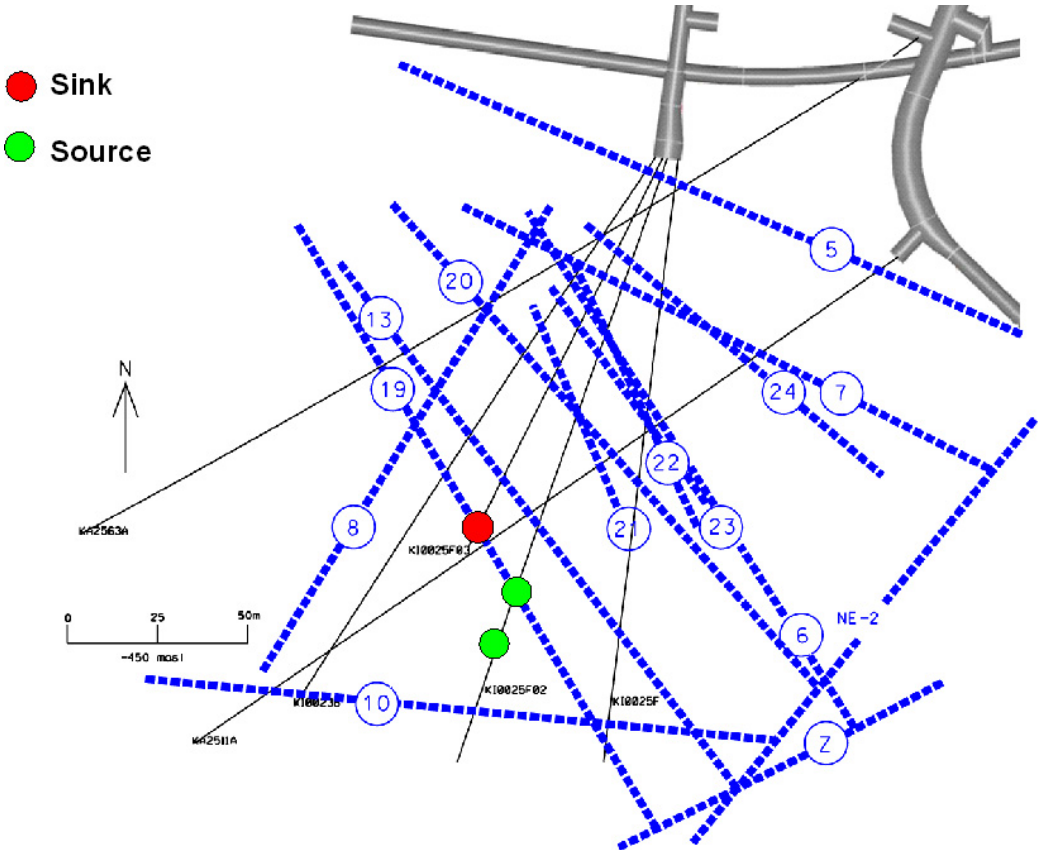

Figure 2-5 *Horizontal section at Z=–450 masl showing structural model based on identified conductive geological structures in the TRUE Block Scale rock volume (Andersson et al. 2002a) and location of injection sections (sources) and pumping section (sink) .*

2.4 Environmental monitoring programme

In previous experiments with sorbing tracers, TRUE Block Scale Phase C (Andersson et al., 2001) samples were taken from a number of positions in the Prototype Repository tunnel, the crossing of the A-tunnel by the I-tunnel and in the I-tunnel, in total six sampling locations. Samples were taken once a week for the first two months and then once every 14th day for the next three months. Results showed no enhanced radioactivity, indicating that tracer is not ending up in the low points made up by the south-western tunnel system.

In the current experiment, the three sampling points OP:1 – OP:3 (see Figure 2-6) are identical with previous sampling points. Sampling point OP:4 is added and three of the previous sampling points have been removed as no visible flow could be detected at these points mainly due to changed pathways in connection to concrete reinforcements. These points were sampled once every 14th day during the course of this experiment to detect any uncontrolled spill of radionuclides to the tunnel. No such spill could be detected.

It should also be noted that the Prototype tunnel has been backfilled since previous experiments at the TRUE Block Scale site. However, the drainage of the tunnel was open during BS2B and no significant effects on flow and pressures could be detected due to the backfill.

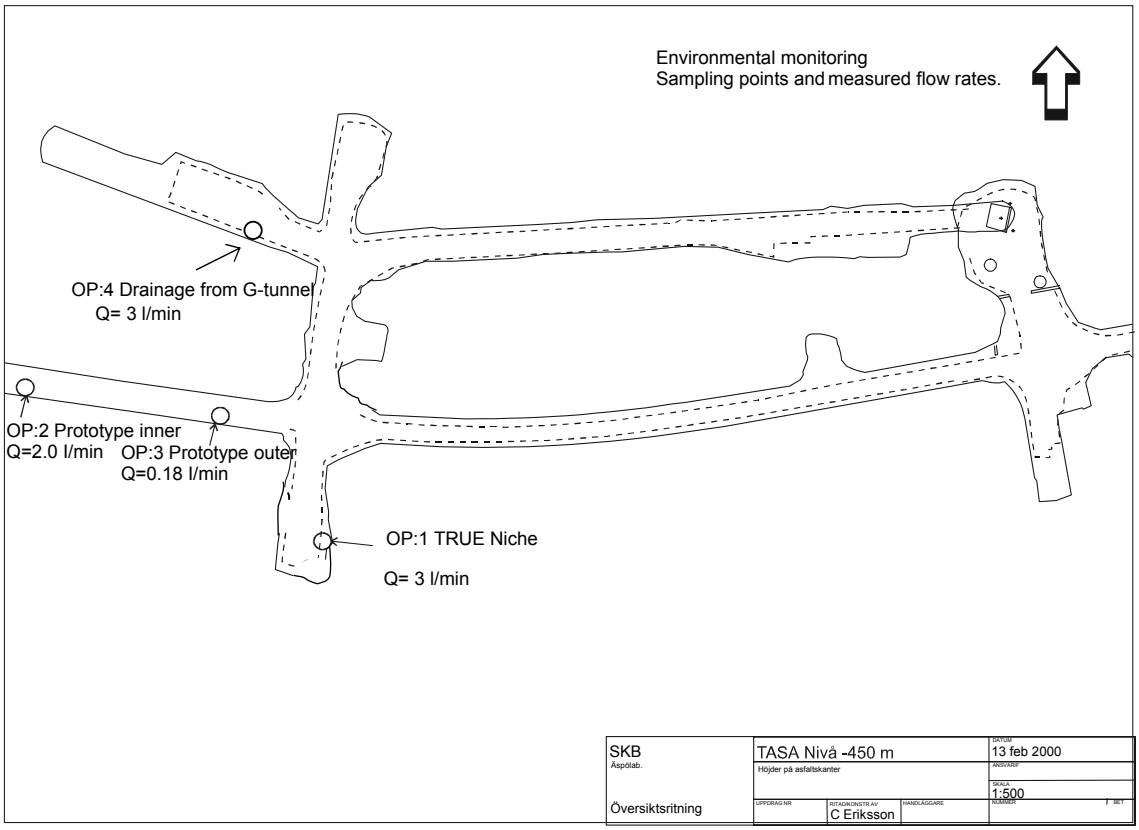

Figure 2-6. *Environmental monitoring sampling points with measured flow rates.*

3 Results and interpretation

3.1 Log of events

In general, the equipment and experimental procedures have worked well and no major hydraulic disturbances have occurred. The only notable disturbance is a pump failure more than 5 months after tracer injection, see Table 3-1. Note that the pumping started already in October 2003, 5 months prior to the BS2B tracer injection, and has not been interrupted at any time.

Table 3-1. Log of events

Date	Event
031006	Start pumping KI0025F03:R3, Q=2.8 l/min (pre-test CPT-4)
040330	Pump flow rate in KI0025F03:R3 has decreased to 2.5 l/min
040330	Start water injection in KI0025F02:R3, 5 ml/min
040331	Start water injection in KI0025F02:R2, 2 ml/min
040331	Start tracer injection in KI0025F02:R3
040331	Start tracer injection in KI0025F02:R2
040820	Pump flow rate in KI0025F03:R3 has decreased to 2.3 l/min
040910	Stop water injection in KI0025F02:R2 (pump failure)
040917	Start water injection in KI0025F02:R2, 2 ml/min
041008	Last sample taken presented in this report

3.1.1 Tracer injections

The injections were performed as decaying pulses with an accompanying injection of non-labelled water in both injection sections. The main reason for adding extra water to the injection was to shorten the tracer residence time in the injection section which is important from a radiation safety aspect when handling radioactive tracers. Long tailing in the injection may also induce tailing in the breakthrough curves which can interfere in the evaluation of the processes.

The measured tracer injection concentrations are presented in Table 3-2 and Figures 3-1 to 3-6. Figures 3-1 to 3-4 shows ensemble plots of all tracer injected in the two flow paths. Both measured values from the discrete sampling (Figures 3-1 and 3-2) and from the on-line measurement cell (Figures 3-3 and 3-4) are displayed. In Figures 3-5 and 3-6 comparison are made between the two measurements (sampling vs on-line) for each tracer. These plots also include error bars representing one standard deviation for the measurements.

In general the on-line measurements give good data at early times when the sampling values are lacking due to a delay in the sampling system (valves and tubing). The delay, estimated to about 4 hours, represents the time it takes to exchange the tubing volume from the circulation loop to the sampler due to the low sampling flow (2 ml/h). A higher sampling flow would decrease the delay but also decrease the injection rate. However, at larger times the delay is not so important and sampled values tend to be more realistic as there is a tendency of sorption in the tubing at the on-line detector possibly caused by precipitations.

Table 3-2. Tracer injection data for TRUE Block Scale Continuation, tests with sorbing tracers. Borehole section notation is shortened by removing the prefix "KI00-" from the borehole label.

Borehole section	Section Volume (ml)*	Inj. rate flow meter (ml/min)	Inj. rate dil.curve (ml/min)	Tracer	$t_{1/2}$	Total Inj. amount (MBq)
F02:R3	7747	5	4.2	$^{131}I^-$	8 d	4.0
				^{160}Tb-DTPA	72.3 d	16
				$^{85}Sr^{2+}$	64.9 d	22
				$^{86}Rb^+$	18.7 d	15
				$^{137}Cs^+$	30.2 y	22
F02:R2	7141	2	1.2	HTO	12.3 y	720
				^{155}Eu-DTPA	4.8 y	5.2
				$^{22}Na^+$	2.6 y	15
				$^{133}Ba^{2+}$	10.5 y	18
				$^{54}Mn^{2+}$	312 d	67

* Section volumes calculated from borehole and equipment specifications.

Based on the concentrations of the non-sorbing radioactive tracers injected, HTO in KI0025F02:R2 and $^{131}I^-$ in KI0025F02:R3, flow rates were calculated from the dilution of tracer versus time (Table 3-2). The calculated values (1.2 and 4.2 ml/min) are both smaller than the actually added flow (2.0 and 5.0 ml/min). This difference has earlier been observed in previous experiments using this set-up and can be explained by poor mixing such that a portion of the unlabelled water added is injected without complete mixing with the rest of the volume in the injection section. This is particularly evident in KI0025F02:R2 where problems with a clogged filter in the borehole equipment only allowed a mixing rate of 2 litres/hour compared to 10 litres/hour in KI0025F02:R3.

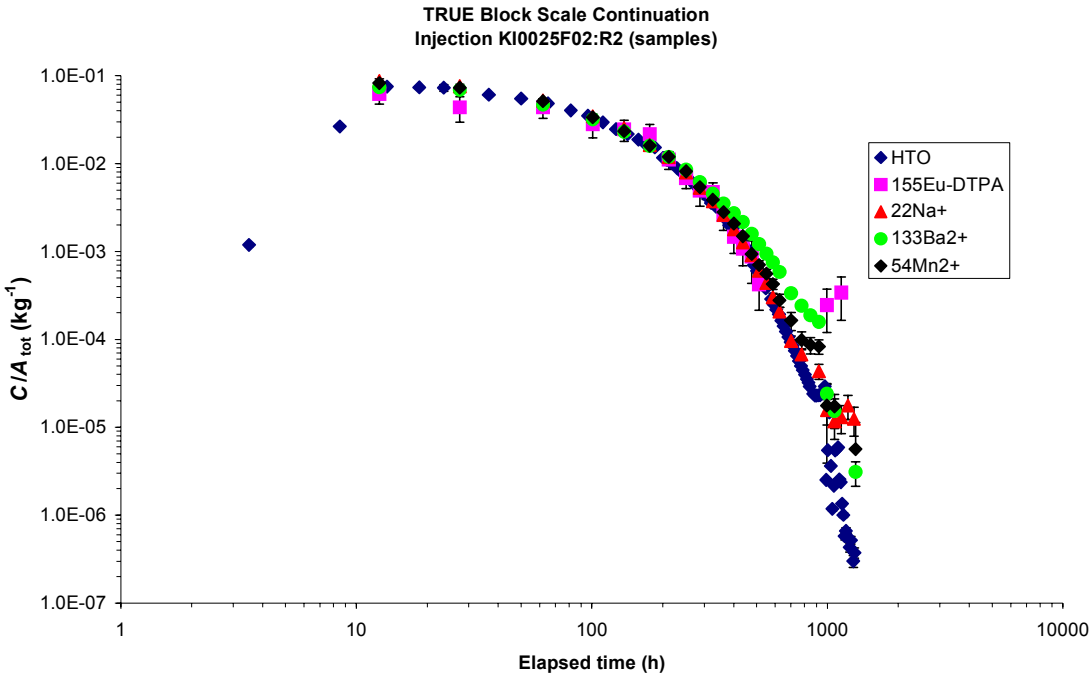

Figure 3-1. *Tracer injection curves (log-log scale) for the injection in KI0025F02:R2 (slow flow path, sample measurements).*

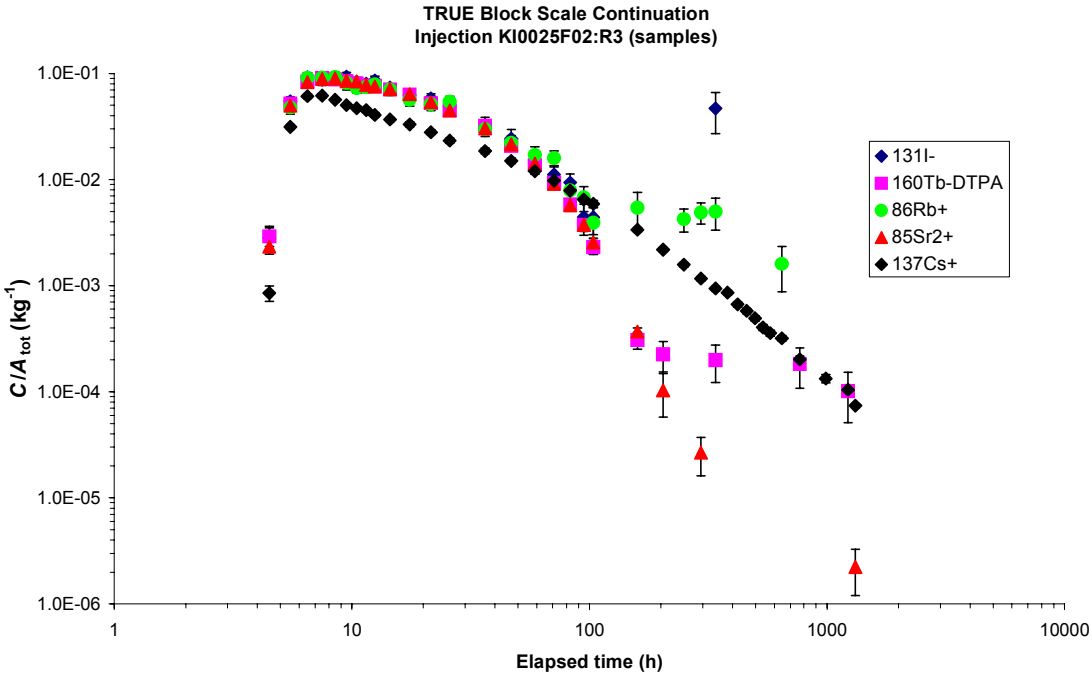

Figure 3-2. *Tracer injection curves (log-log scale) for the injection in KI0025F02:R3 (fast flow path, sample measurements).*

Figure 3-1 shows good agreement between the he measured concentrations (activities) of discrete samples taken from the tracer injection loop for most of the tracers. A small tendency of higher relative concentrations for the sorbing tracers can be noted, especially at longer times. This effect is much more pronounced in the injection interval for the fast flow path (Figure 3-2) where sorption effects are clearly visible for both $^{86}Rb^{+}$ and $^{137}Cs^{+}$.

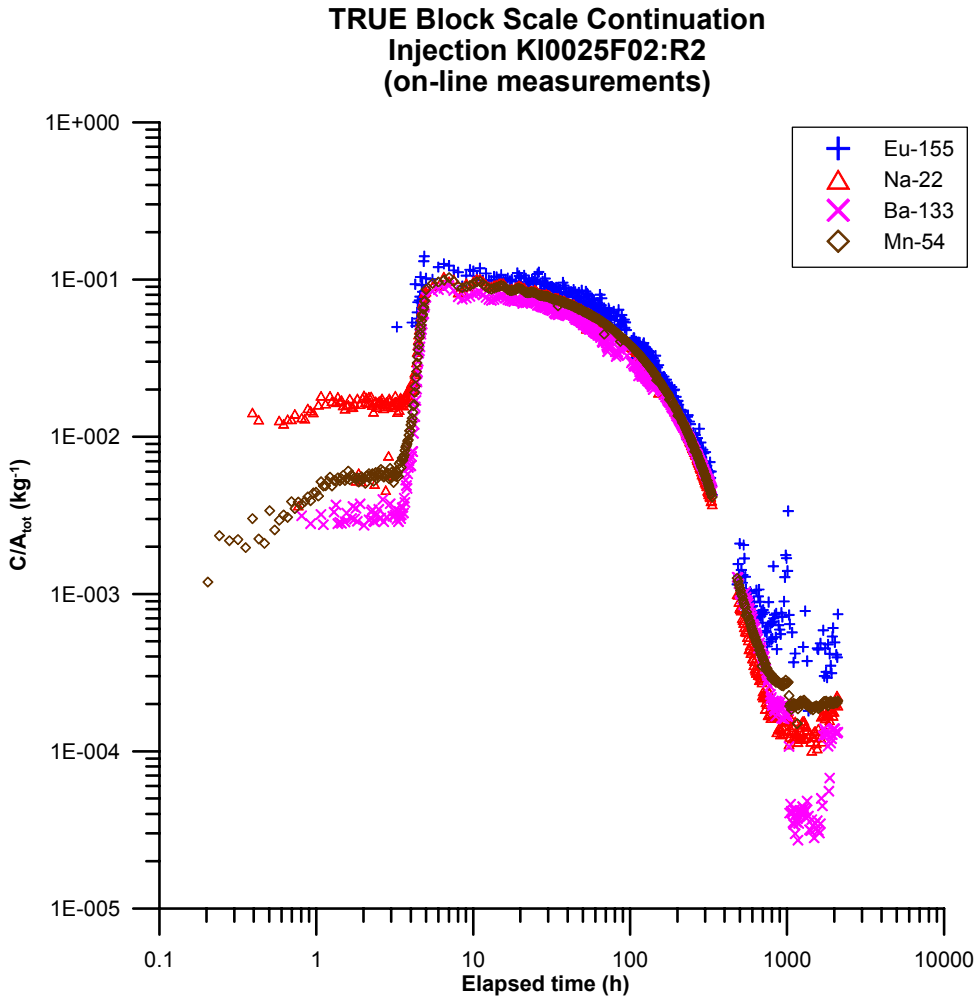

Figure 3-3. *Tracer injection curves (log-log scale) for the injection in KI0025F02:R2 (slow flow path, on-line measurements).*

Notable in the on-line measurement (Figure 3-3) is the relatively poor mixing in KI0025F02:R2 due to the low mixing rate. The injection concentration does not rise until about 4 hours and varies somewhat during quite a long time (about 25 h).

In the early on-line injection data for the slow flow path (KI0025F02:R2), it is indicated that the relative concentration of $^{22}Na^{+}$ at the first injection phase is almost one order of magnitude higher than the other tracers (Figure 3-3). However, this is caused by the fact that the on line γ-spectrometry detector is in close vicinity to the injection pump which cause disturbance in the measurements. The γ-radiation from $^{22}Na^{+}$ has the highest γ-energy of the tracers used which favours the γ-radiation penetration through the lead shielding and into the detector.

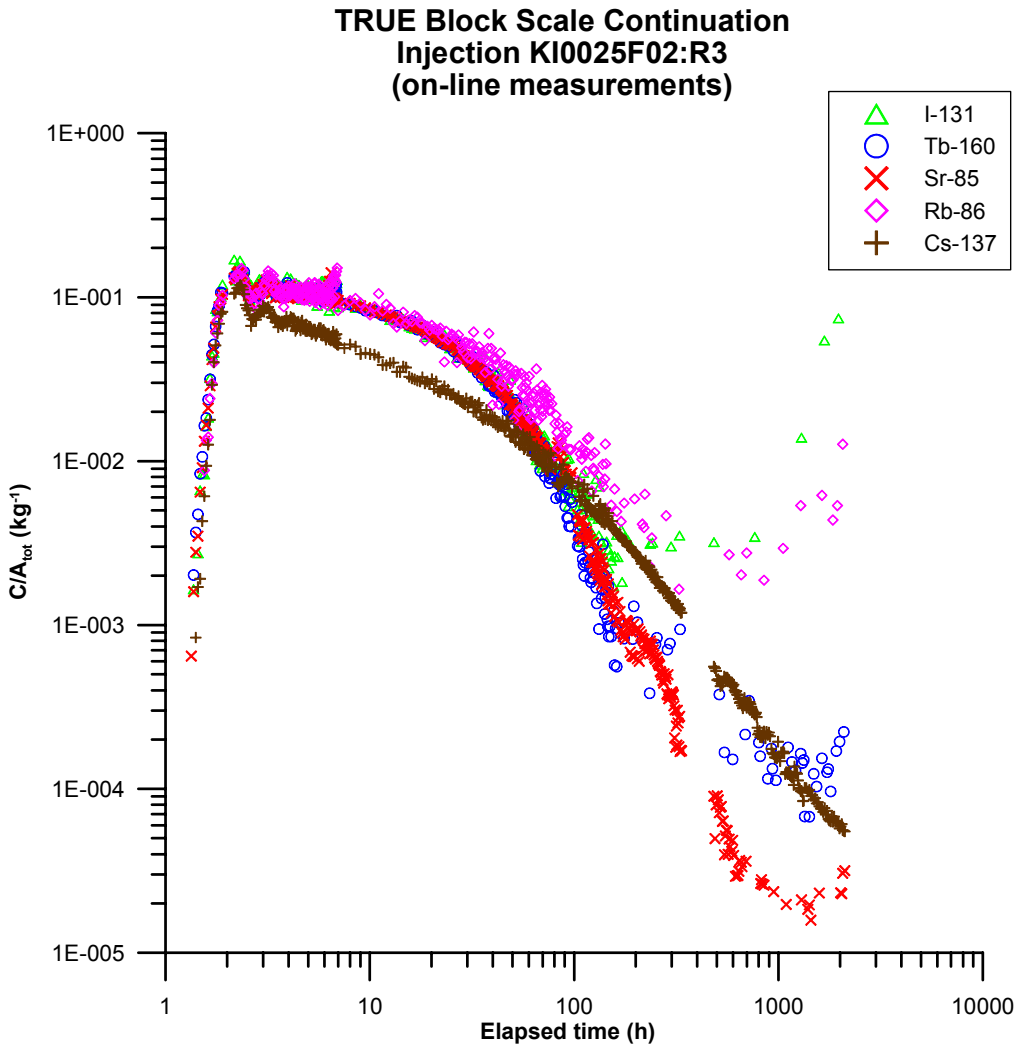

Figure 3-4. *Tracer injection curves (log-log scale) for the injection in KI0025F02:R3 (fast flow path, on-line measurements).*

The on-line measurements in the injection interval for the fast flow path (Figure 3-4) gives a much more correct picture of the initial mixing and should therefore be used as input when evaluating the breakthrough curve. Some data points indicating a rise in the injection curve at the late times can be observed for the most short-lived tracers used, i.e., $^{131}I^-$ and $^{86}Rb^+$. However, these data points are associated with large measurement errors. Furthermore, a careful inspection of the γ-spectrometry data has raised doubt of the existence of any peak above the background level in these cases. Nevertheless, the automated γ-spectrometry evaluation routine claims the existence of a peak. This problem has been reported to the manufacture of the program.

Due to the combination of a long time elapsed since the injection (the reference time) and the short half-life of the tracers, the decay correction give very high concentrations. However, one should be aware of that between these few data points that indicate high concentrations there are several measurements where the tracer concentrations have been found to be below the detection limits.

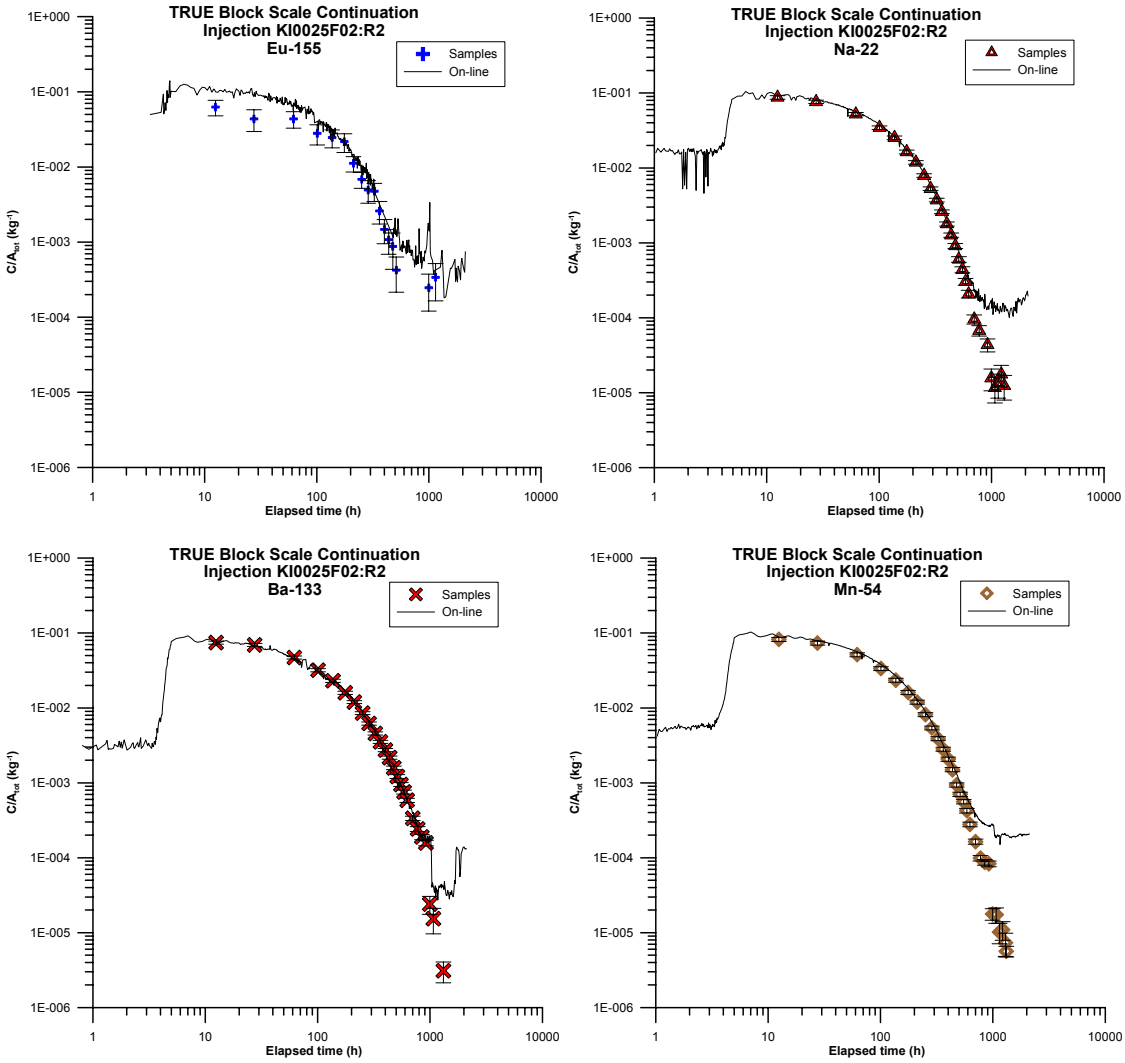

Figure 3-5. *Comparison between on-line measurements and samples for tracers used in the slow flow path (injection in KI0025F02:R2). Error bars represent one standard deviation.*

Figures 3-5 and 3-6 show comparisons between on-line measurements and sampling for each tracer, except HTO where only sampling was applied. The graphs clearly show the usefulness of on-line data at early times whereas late-time data generally are better represented by samples.

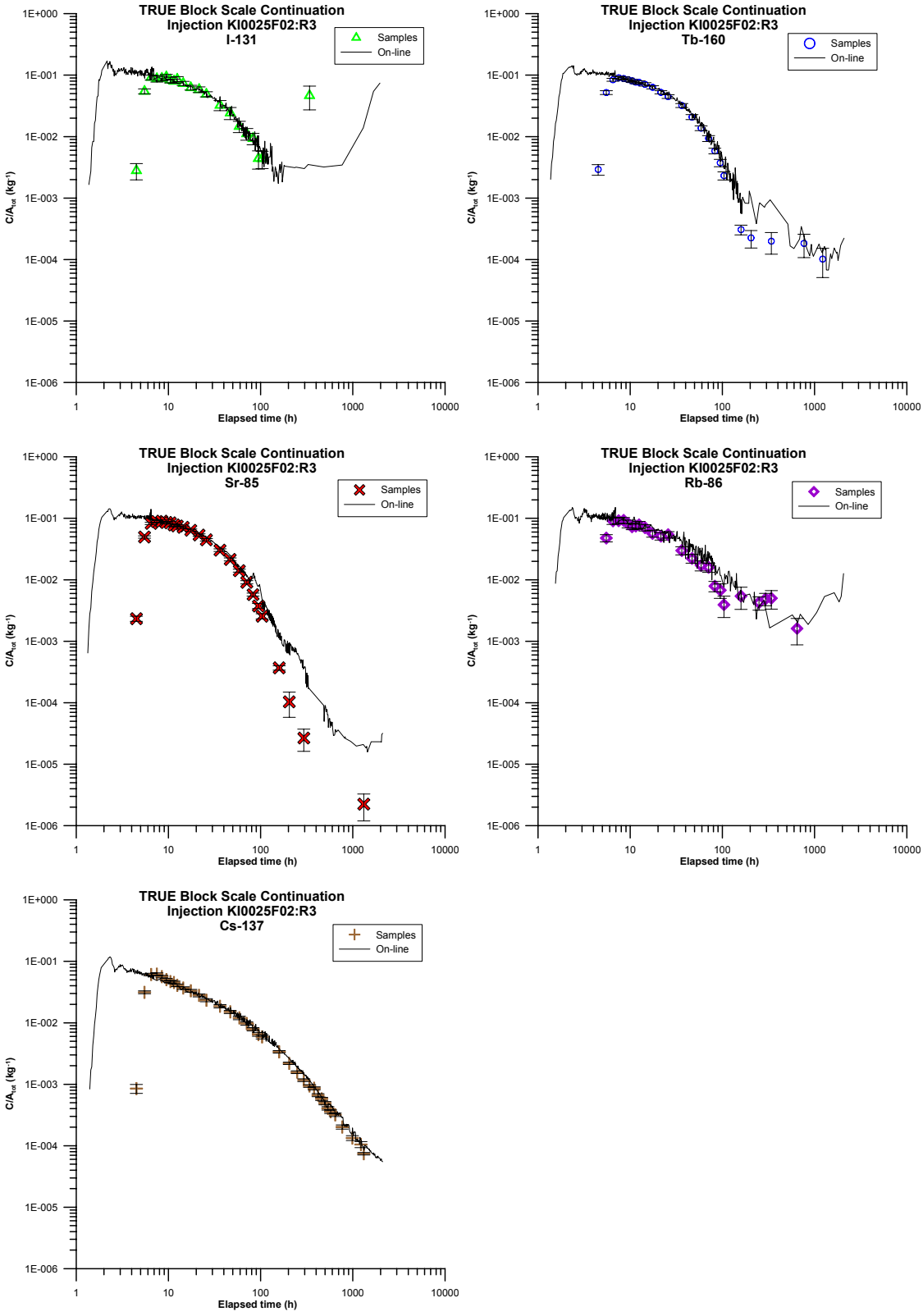

Figure 3-6. *Comparison between on-line measurements and samples for tracers used in the fast flow path (injection in KI0025F02:R3). Error bars represent one standard deviation.*

3.1.2 Tracer breakthrough

Tracer breakthrough in the sink section KI0025F03:R3 (Structure #19) was detected for all tracers injected in both injection sections, KI0025F02:R3 (Structure #19) and KI0025F02:R2 (BG#1), cf. Figure 3-7 and 3-8, respectively. The tracer mass recovery was high for the non-sorbing and weakly sorbing tracers, cf. Table 3-3 and 3-4.

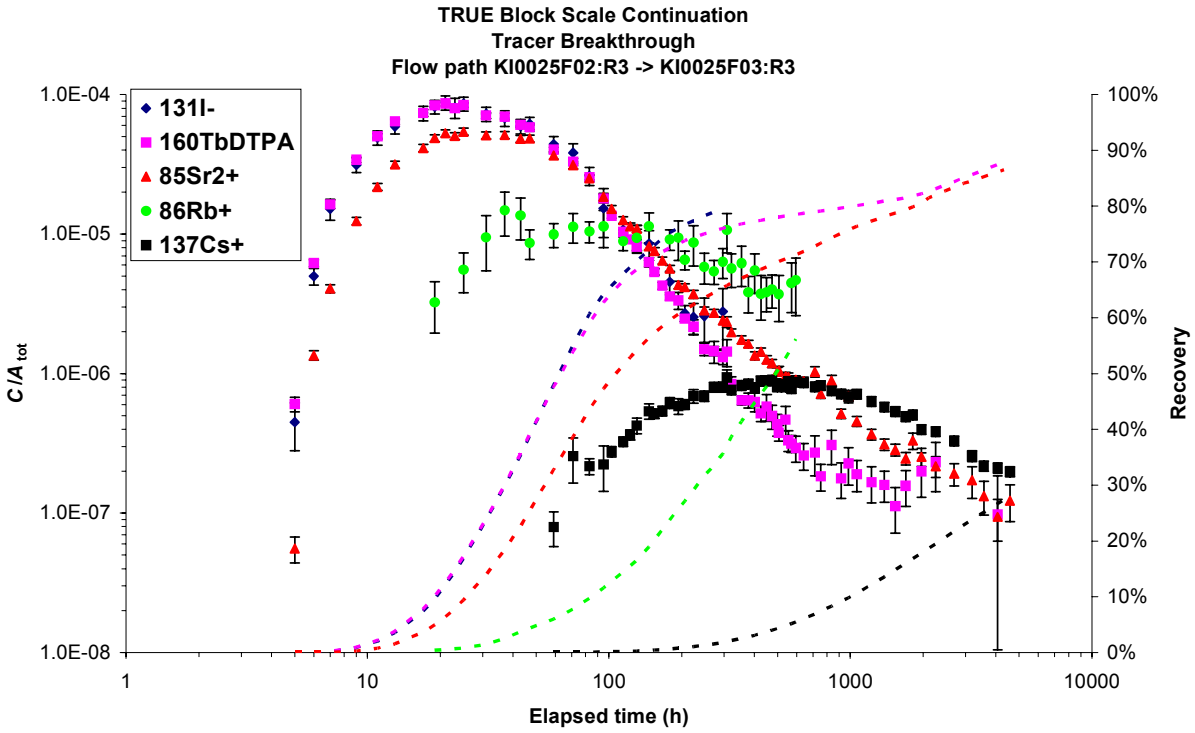

Figure 3-7. *Tracer breakthrough curves and mass recovery for TRUE Block Scale Continuation BS2B tests with sorbing tracers, injection in KI0025F02:R3 (log-log scale). Concentrations are normalised to injected mass. Error bars represent one standard deviation.*

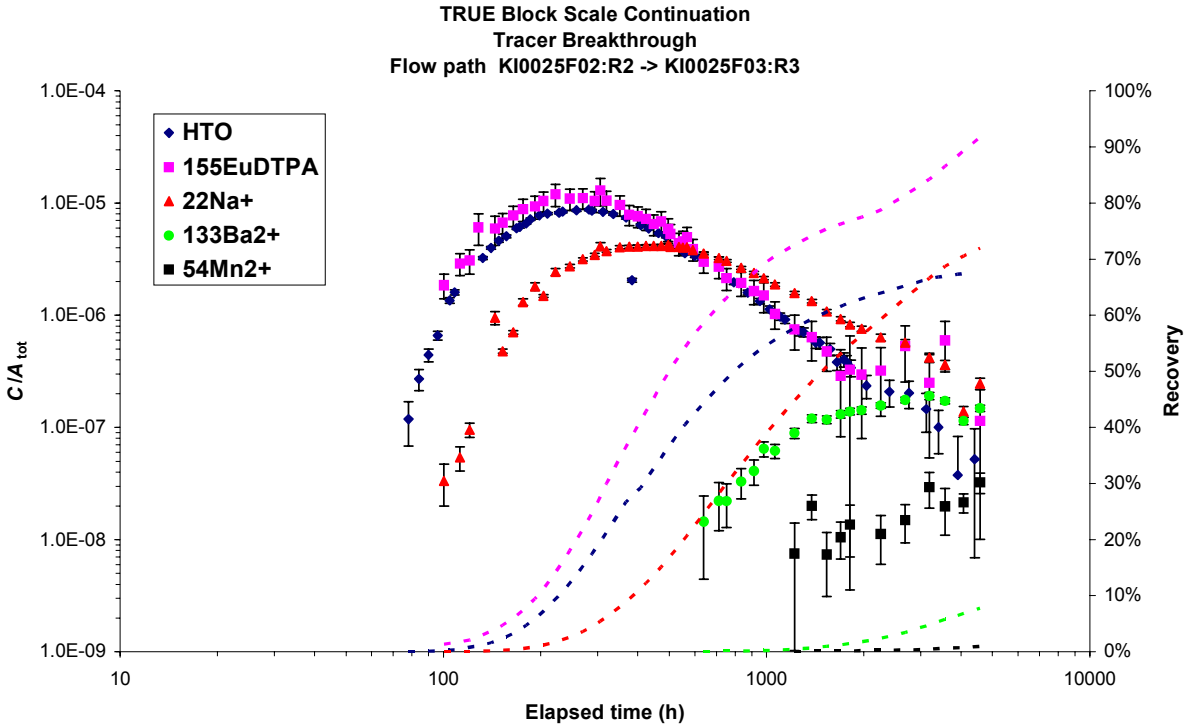

Figure 3-8. *Tracer breakthrough curves and mass recovery for TRUE Block Scale Continuation BS2B tests with sorbing tracers, injection in KI0025F02:R2 (log-log scale). Concentrations are normalised to injected mass. Error bars represent one standard deviation.*

Tracer mass recovery was calculated in the same way for all tracers detected in the pumping section. Before the injection a sample of the stock solution was taken and the tracer solution vessel was weighed. After the injection the vessel was weighed again and the tracer concentrations of the stock solution sample were measured to determine the injected mass of the different tracers, cf. Table 3-2. The tracer mass recovered in the pumping borehole section was determined by integration of the breakthrough curves for mass flux (Bq/h) versus time (h).

The mass recovery is high for the non-sorbing tracers in both flow paths and similar to the ones obtained in the pre-tests (Andersson et al., 2004). Pre-test CPT-4c gave a mass recovery of 84% for the fast flow path and 80% for the slow flow path. This is somewhat lower than the ones reported for the DTPA-complexes in Tables 3-3 and 3-4 but the sampling time is also about 10 times longer for the latter. The mass recovery for HTO is much lower than expected and there is currently no explanation for this.

Tracer travel times, t_5, t_{50} and t_{95} (defined as times when 5, 50 and 95 % of the recovered mass has arrived in the pumping section at the stop time of sampling, t_t) were calculated and are presented together with the total mass recovery (calculated at the stop time of sampling, t_t) in Tables 3-3 and 3-4. Notable here is the significant difference between the two non-sorbing tracers in the slow flow path, ^{155}Eu-DTPA and HTO.

Table 3-3. TRUE Block Scale Continuation, BS2B, flow path KI0025F02:R3 – KI0025F03:R3 (fast flow path). Tracer travel times, t_5, t_{50} and t_{95} and tracer mass recovery at t_t (t_t is the time for the last sample taken).

Tracer	t5 (h)	t50 (h)	t95 (h)	tt (h)	Recovery (%)
131I-	14	62	-	296	80
160Tb-DTPA	14	63	-	4075	87
85Sr2+	19	107	-	4327	86
86Rb+	51	490	-	594	56
137Cs+	555	-	-	4579	28

Table 3-4. TRUE Block Scale Continuation, BS2B, flow path KI0025F02:R2 – KI0025F03:R3 (slow flow path). Tracer travel times, t_5, t_{50} and t_{95} and tracer mass recovery at t_t (t_t is the time for the last sample taken).

Tracer	t_5 (h)	t_{50} (h)	t_{95} (h)	t_t (h)	Recovery (%)
HTO	183	790	-	4409	68
^{155}Eu-DTPA	155	500	-	4577	92
$^{22}Na^{+}$	300	1490	-	4577	72
$^{133}Ba^{2+}$	3250	-	-	4577	8
$^{54}Mn^{2+}$	-	-	-	4577	1

3.2 Supporting data

The tests were performed by pumping in KI0025F03:R3 (Structure #19) using a withdrawal rate of Q=2.5 l/min at the start of the tracer injections, March 31st , 2004, slowly decreasing to Q=2.3 l/min at the end of the test period, October 8th, 2004, c.f. Figure 3-9. During the first 1000 hours, where most of the mass transport occurs, flow decreased from 2.52 to 2.48 l/min.

The head distribution in the sink section (KI0025F03:R3) and injection sections, KI0025F02:R2 (BG#1) and KI0025F02:R3 (Structure #19), during the test period is shown in Figure 3-10. A slowly decreasing pressure trend in the sink section, is clearly seen indicating restrictions in the flow system (i.e. a no-flow boundary). The decrease in head in section KI0025F02:R2 during a week in September occurred when the water injection was stopped due to a pump failure.

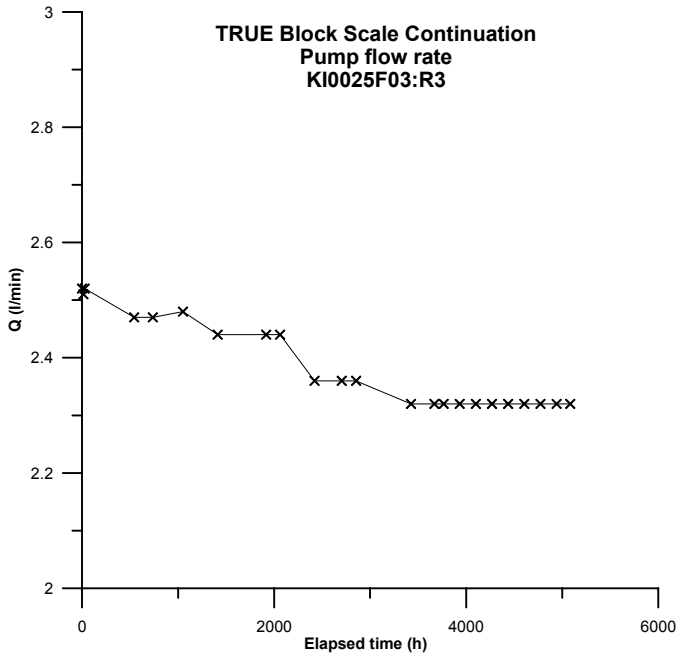

Figure 3-9. *Pump flow rate in KI0025F03:R3 versus time elapsed since start of tracer injection.*

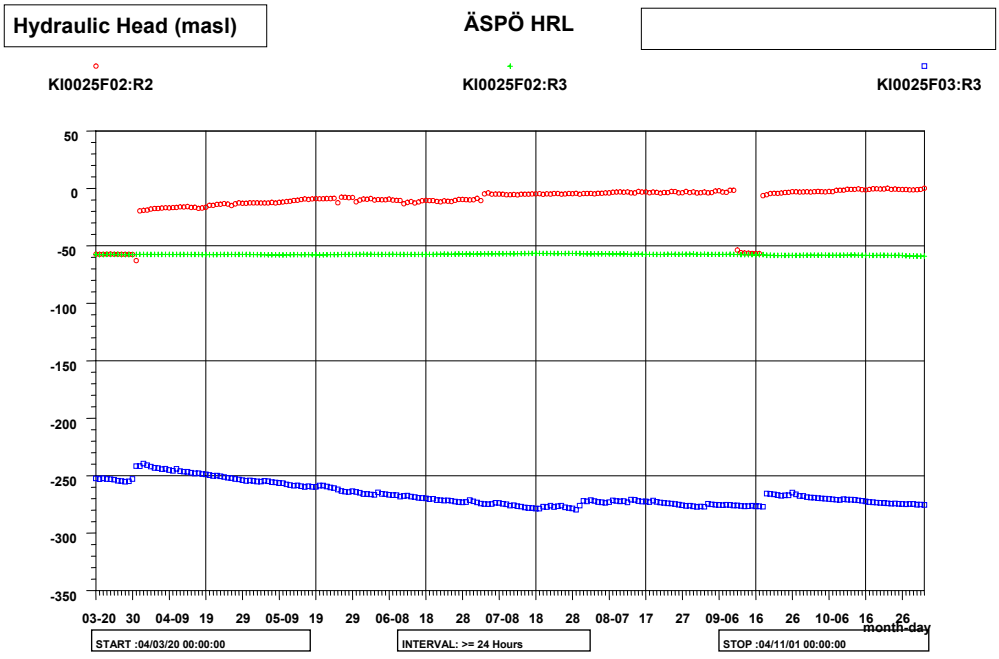

Figure 3-10. *Hydraulic head in source sections KI0025F02:R2 (Structure #25) and KI0025F02:R3 (Structure #19) and sink section KI0025F03:R3 (Structure #19) during TRUE Block Scale Continuation BS2B tests with sorbing tracers.*

4 Model evaluation of tracer breakthrough

4.1 General

Evaluation of the tracer breakthrough curves has been made by performing parameter estimation using three basic one-dimensional models:

- Advection-dispersion model with a single transport pathway.
- D:o with two separate transport pathways.
- Advection-dispersion model with matrix diffusion and equilibrium sorption

These models have been fitted to the experimental tracer breakthrough curves by non-linear least squares regression.

4.2 Transport models

Advection-dispersion model in a single pathway (AD-1)

This model is described by the standard governing equation for one-dimensional advection-dispersion transport:

$$a_L v \frac{\partial^2 C}{\partial x^2} - v \frac{\partial C}{\partial x} = \frac{\partial C}{\partial t} \qquad (4\text{-}1)$$

where C is concentration (e.g. M/L^3), x is distance along transport path (L), t is time (T), v is the average water velocity (L/T) and a_L is the longitudinal dispersivity (L).

The following initial and boundary conditions are applied:

$$C(x,t) = 0 \qquad t = 0 \qquad (4\text{-}2)$$

$$\frac{\partial C(x,t)}{\partial x} = 0 \qquad x = \infty \qquad (4\text{-}3)$$

$$-a_L v \frac{\partial C}{\partial x} + vC = C_0 \qquad x = 0 \qquad (4\text{-}4)$$

The above boundary and initial conditions results in a solution for a constant injection of tracer. For a tracer injection pulse with constant concentration of limited duration (t_{inj}), the resulting tracer concentration may be calculated as:

$$C(x,t) = M(x,t) \qquad 0 < t \leq t_{inj} \qquad (4\text{-}5)$$

$$C(x,t) = M(x,t) - M(x, t - t_{inj}) \qquad t > t_{inj} \qquad (4\text{-}6)$$

where $M(x,t)$ is the solution for a step-input injection with constant injection concentration. A more complex temporal variation in the tracer injection may be calculated in an analogous way by summation of a several such injection periods. Solutions of the above equations are given by, for example, Javandel et al (1984).

Advection-dispersion model in two pathways (AD-2)

This model is essentially the same as the preceding one (AD-1) except that tracer transport is assumed to occur in two separate pathways and mix in the pumping section. This is calculated by summing the contribution from the different pathways as (for n pathways:

$$C(x,t) = \sum_{i=1}^{n} pf_i \cdot C_i(x,t) \tag{4-7}$$

where $C_i(x,t,)$ represents the partial tracer breakthrough from each individual pathway and pf_i is a proportionality factor that describes the contribution from each pathway.

It may here also be noted that the pf parameter also represents dilution effects in the pumping section as well as other proportional tracer losses. Thus, this parameter is often relevant to include also when applying the AD-1 model.

Advection-dispersion model with matrix diffusion and equilibrium sorption

In this model, the governing equation for the AD model is extended by adding a term that represents diffusion of tracer into a hydraulically stagnant matrix:

$$R_a \frac{\partial C}{\partial t} = - v \frac{\partial C}{\partial x} + a_L v \frac{\partial^2 C}{\partial x^2} + \frac{2 D_e}{\delta} \frac{\partial C_p}{\partial y} \tag{4-8}$$

with the transport in the matrix given by:

$$\frac{\partial C_p}{\partial t} - \frac{D_e}{R_d n_p} \frac{\partial^2 C_p}{\partial y^2} = 0 \tag{4-9}$$

where n_p is the matrix porosity, D_e is the effective diffusion coefficient (L^2/T), δ is the fracture aperture (L) of the flowing fracture, $C_p\ (y)$ is the tracer concentration in the matrix, R_a is the linear retardation factor in the fracture, R_d is the linear retardation factor in the matrix and y is a spatial coordinate perpendicular to the direction of the flowing transport path. The matrix diffusion model used here is also presented by Tang et al. (1981) and Moreno et al. (1985).

When this matrix diffusion model is employed for interpretation of tracer breakthrough curves, all unknown parameters in equations (4-8) and (4-9) can not be evaluated independently. Instead, one may use a lumped parameter, A, which describes the effect of matrix diffusion. The parameter A may be written as:

$$A = \frac{\delta R_a}{2\sqrt{n_p R_d D_e}} \tag{4-10}$$

With this definition, the matrix diffusion effect increases with decreasing values of A.

Based on estimated values of the residence time (t_0) and other information about flow rates, heads, etc, other parameters may be derived assuming radial flow in a homogenous fracture. The equivalent hydraulic fracture conductivity, $K_{fr,}$ may be calculated using:

$$K_{fr} = \ln(\frac{r}{r_w}) \cdot \frac{r^2 - r_w^{\ 2}}{2t_0 \Delta h} \tag{4-11}$$

where r is the travel distance [L], r_w is the borehole radius [L], t_0 is the average travel time [T], and Δh is the head difference [L] between the injection and the pumping section.

The equivalent fracture aperture, δ [L], may be calculated as:

$$\delta = \frac{Q_{bh} t_0}{\pi(r^2 - r_w^{\ 2})} \tag{4-12}$$

where Q_{bh} is the pumping rate [L^3/T].

4.3 Parameter estimation method

Parameter estimates are obtained using weighted non-linear least-squares regression. The basic non-linear least-squares regression algorithm minimises the sum of squared differences between the modelled (Y^M) and the observed (Y^O) variables and may be formulated as:

$$\text{Min } S = \mathbf{E_R}^T \mathbf{W} \mathbf{E_R} \tag{4-13}$$

where $\mathbf{E_R}$ is a vector of residuals ($\mathbf{Y}^M - \mathbf{Y}^O$) and $\mathbf{W}$ is a vector of reliability weights on observations.

The specific method for carrying out the regression employed in this study is often referred to as the Marquardt-Levenberg method (Marquadt (1963), Levenberg (1944)). This method is a Newton-type optimisation algorithm that finds the parameter values that minimises the sum of squared errors between model and measurement values in an iterative manner. A simplified version of the search algorithm used may be written as:

$$\mathbf{B}_{r+1} = \mathbf{B}_r + (\mathbf{X}_r^T \mathbf{W} \mathbf{X}_r)^{-1} \mathbf{X}_r^T (\mathbf{Y}^O - \mathbf{Y}_r^M) \tag{4-14}$$

where $\mathbf{B}$ is a vector of parameter estimates, $\mathbf{X}$ is a parameter sensitivity matrix, and the subscripts r and $r+1$ refer to the iteration number.

Given an initial parameter estimate, eq. (4-12) is repeated until a local optimal solution is found. The local minimum is defined by some convergence criterion, for example when parameter estimates are essentially identical between iterations. Finding a local minimum does not guarantee that the global minimum is found. When this appears to be a problem, several sets of initial estimates may be tried. When some knowledge about the parameters to be estimated and the physical system is already available, the initial estimates are often good enough for ensuring that a global minimum is found.

An important element of the above procedure is the matrix containing the parameter sensitivities. Parameter sensitivity is defined as the partial derivative of the dependent (simulated) variable with respect to a parameter. A sensitivity matrix contains one row for each observation and one column for each estimated parameter, as in the following example with three observations and two parameters.

$$\mathbf{X} = \begin{pmatrix} \frac{\partial y_1}{\partial b_1} & \frac{\partial y_1}{\partial b_2} \\ \frac{\partial y_2}{\partial b_1} & \frac{\partial y_2}{\partial b_2} \\ \frac{\partial y_3}{\partial b_1} & \frac{\partial y_3}{\partial b_2} \end{pmatrix} \tag{4-15}$$

In this report, multiple data sets (tracer breakthrough curves) are used simultaneously in regression for evaluating sorbing tracers. This requires a somewhat modified sensitivity matrix, but is fairly straight-forward to implement.

The model analysis involves weighted regression which means that each observation is assigned a weight. The weights are often thought of as a reliability measure so that more uncertain observations are made less important in the regression procedure. Additionally, the weights may simply be regarded as a means to emphasize/de-emphasize any part of the observation data. In this report, weights are derived using the analysis uncertainty provided with the experimental breakthrough data. The analysis uncertainty is for most of the tracers roughly proportional to the observation data, and this has the effect of making low concentration values important in the regression analysis. More importantly, this choice of weights will also automatically provide suitable weights for the regression on multiple data sets (for the sorbing tracers).

Parameter sensitivities may be used to determine the precision of the estimated parameter values. Given below are two diagnostic measures regarding parameter uncertainty that may be obtained as a result of regression (Cooley, 1979).

The *standard errors* of parameter estimates are obtained by taking the square roots of the diagonals in the parameter covariance matrix, which is given by:

$$s^2(\mathbf{X}^\mathbf{T}\mathbf{W}\mathbf{X})^{-1} \tag{4-16}$$

with s^2 being the error variance

$$s^2 = \frac{\sum_{i=1}^{N} w_i \, (y_i^O - y_i^M)^2}{N - P} \tag{4-17}$$

where N is the number of measurements, P the number of parameters and w_i the weight on observation i.

The linear correlation $r(p_1,p_2)$ between two parameters p_1 and p_2 is expressed by:

$$r(p_1, p_2) = \frac{\mathrm{Cov}(p_1, p_2)}{\sqrt{\mathrm{Var}(p_1)\,\mathrm{Var}(p_2)}} \tag{4-18}$$

where the variance and covariance terms are elements of the $s^2(\mathbf{X^T W X})^{-1}$ matrix. The correlation is a measure of the inter-dependence between two parameter estimates and correlation values range between –1 and 1. Values close to either –1 or 1 mean that a change in one parameter value may be compensated for by a change in another parameter value to maintain the same fit (sum of squares) between model and measurements.

The standard errors and parameter correlation values are the main diagnostic measures used in this analysis when examining the parameter estimation results from evaluation of the tracer tests. In Section 4.6.2, parameter estimates are presented along with an estimation uncertainty for each parameter. This uncertainty is herein expressed as the *coefficient of variation* and is for a parameter estimate p_i calculated as:

$$CV(p_i) = \frac{s.e.(p_i)}{p_i} \tag{4-19}$$

where $s.e.(p_i)$ is the standard error for parameter *I,* as defined in Section 4.3. Thus, the estimation error is expressed as a fraction of the estimated value.

4.4 Handling of injection data

Tracer injections were made as decaying pulse injections, i.e. injection of a tracer pulse in a re-circulating system. The injections were also accompanied by net fluid injections into the injection section. A simple and reasonable assumption is that the amount of tracer that leaves the injection section (and into the transport part) is proportional to the tracer concentration in the injection section.

Injection functions are given as a stepwise input function to the model. This function is mostly based on analysed samples from the injection. However, early values close to the start of the injection are estimated from the on-line measurements, because delay in the sampling system results in non-representative tracer injection samples at early times. This is especially important for the faster of the flow paths, where the time scale of the injection is on the same order of magnitude as for the tracer breakthrough. For the slower transport path, on the other hand, model results are much less sensitive to the injection.

4.5 Calculation of theoretical recovery

Theoretical tracer recovery is in this report calculated as follows:

$$Recovery(\%) = 100x\frac{Q_w}{M_{inj}}\int_0^\infty C^{mod}(t)dt \tag{4-20}$$

where Q_w is the flow rate from the sampling section. The tracer recovery is obtained by integrating the best-fit model breakthrough curve. The model concentration, C^{mod}, may be used when there is a reasonably good agreement between model and field measurements (i.e. reasonably small systematic errors in the model fit). The advantages of this are that the model breakthrough curve may be extended so that a complete recovery may be calculated, and that the model curve provides a filter for measurement noise.

4.6 Results

4.6.1 Estimation parameters

The following parameters were estimated for each model:

- AD-1: t_0 (residence time), a_L (longitudinal dispersivity), *pf* (proportionality factor).
- AD-2*:* t_{01}, $a_{L,1}$, pf_1 (pathway 1); t_{02}, $a_{L,2}$, pf_2 (pathway 2).
- MD: t_0, a_L, *pf*, *A* (matrix diffusion parameter).
- Simultaneous fitting of more than one tracer was carried out using the MD model. In this case, *v* and a_L are common parameters for all tracers, *pf* and *A* are estimated for each tracer, and *R* (retardation factor) is estimated for the sorbing tracer(s).

As was mentioned above, the parameter pf also represents dilution effects in the sampling section. Thus, this parameter may be included in the model fitting even if only one transport path is considered. For a single transport pathway and where the function $C_0\ (t)$ (injection concentration) is known, *pf* may be expressed as:

$$\mathrm{pf} = \frac{\mathrm{Q_{inj}}}{\mathrm{Q_w}} \cdot \mathrm{loss\,factor} \qquad (4\text{-}21)$$

where Q_{in} is the flow rate leaving the injection section and Q_w is the pumping flow rate in the sampling section.

The injection function $C_0(t)$ is often known only with uncertainty. In addition, the parameter *pf* may also be used to account for miscellaneous proportional losses such as sorption of tracer on equipment. Thus, the parameter *pf* should be regarded as a composite parameter accounting for dilution, uncertainty in tracer injection, other proportional tracer losses, and, in the cases of more than one transport pathway, also as a distribution factor for each pathway.

4.6.2 Flow path KI0025F02:R2 - KI0025F03:R3

Non-sorbing tracers

Non-sorbing tracers for this flow path were HTO and ^{155}Eu-DTPA. The breakthrough curves for both of these tracers were analysed using the AD (advection-dispersion; see Section 4.2) and MD (advection-dispersion with matrix diffusion; see Section 4.2) models. The results are summarised in Table 4-1 and the model fits are shown in Figures 4-1 and 4-2 for HTO and ^{155}Eu-DTPA, respectively.

Table 4-1. Parameter estimation results for non-sorbing tracers for flow path KI0025F02:R2 - KI0025F03:R3 (slow flow path). Estimation errors expressed as coefficient of variation are given within parentheses.

Model	Parameter	Units	HTO		^{155}Eu-DTPA	
AD-1	t_0	H	276	(0.03)	268	(0.03)
	a_L	M	6.4	(0.06)	10.4	(0.11)
	pf		$5.0 \cdot 10^{-4}$	(0.03)	$6.5 \cdot 10^{-4}$	(0.04)
AD-2	$t_{0,1}$	H	193	(0.03)	195	(0.15)
	$a_{L,1}$	M	2.7	(0.23)	3.6	(0.15)
	pf_1		$2.5 \cdot 10^{-4}$	(0.44)	$4.9 \cdot 10^{-4}$	(0.31)
	$t_{0,2}$	H	522	(0.41)	772	(0.60)
	$a_{L,2}$	M	10.0	(1.05)	6.5	(1.92)
	pf_2		$3.1 \cdot 10^{-4}$	(0.38)	$2.3 \cdot 10^{-4}$	(0.71)
MD	t_0	H	144	(0.04)	177	(0.14)
	a_L	m	1.6	(0.08)	2.8	(0.24)
	pf		$6.8 \cdot 10^{-4}$	(0.01)	$8.2 \cdot 10^{-4}$	(0.03)
	A	$S^{½}$	559	(0.07)	893	(0.24)

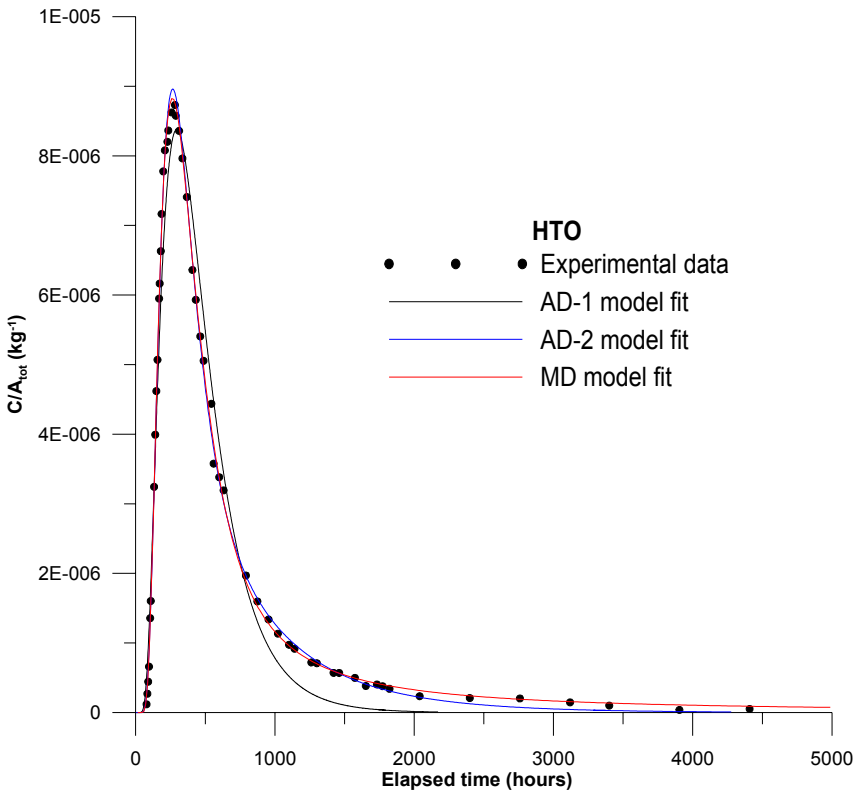

***Figure 4-1a**. Linear plot of model fits for HTO.*

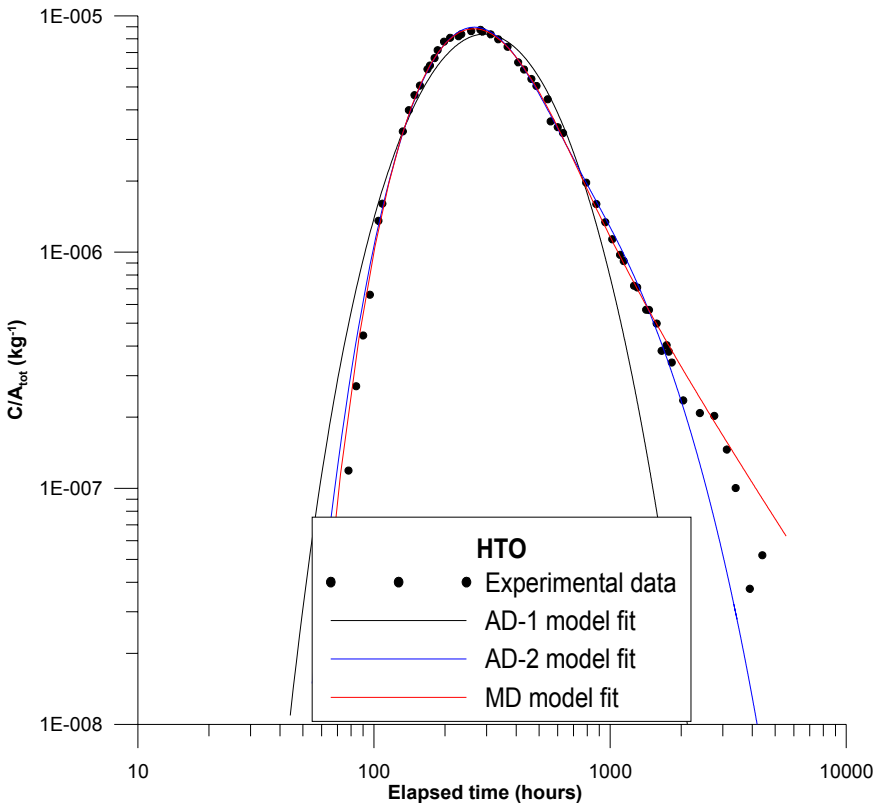

***Figure 4-1b**. Logarithmic plot of model fits for HTO.*

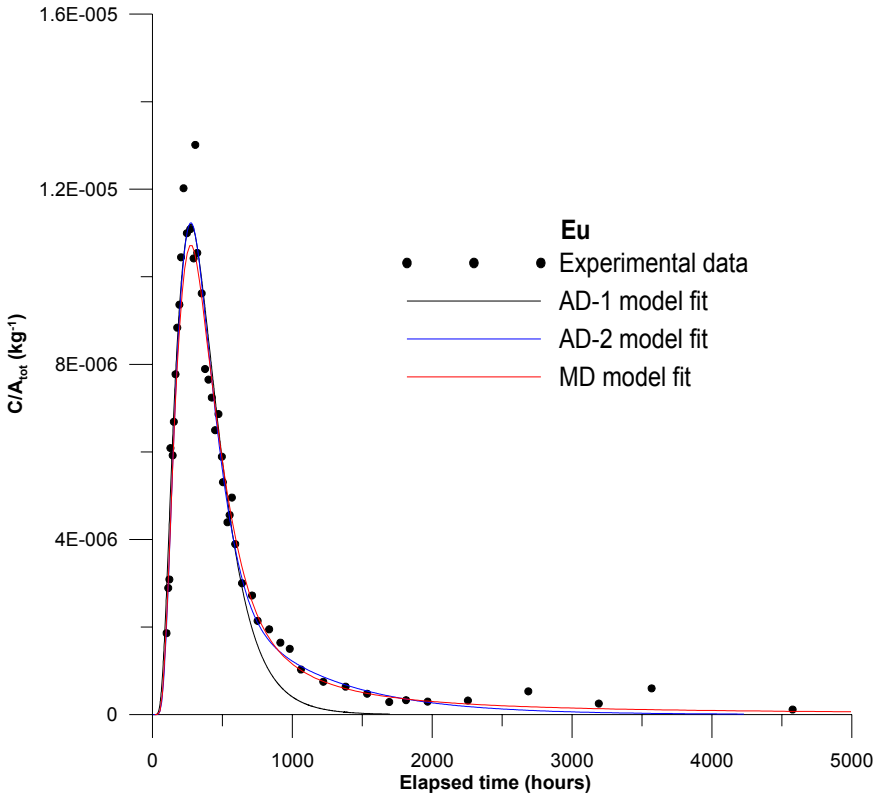

***Figure 4-2a**. Linear plot of model fits for ^{155}Eu-DTPA .*

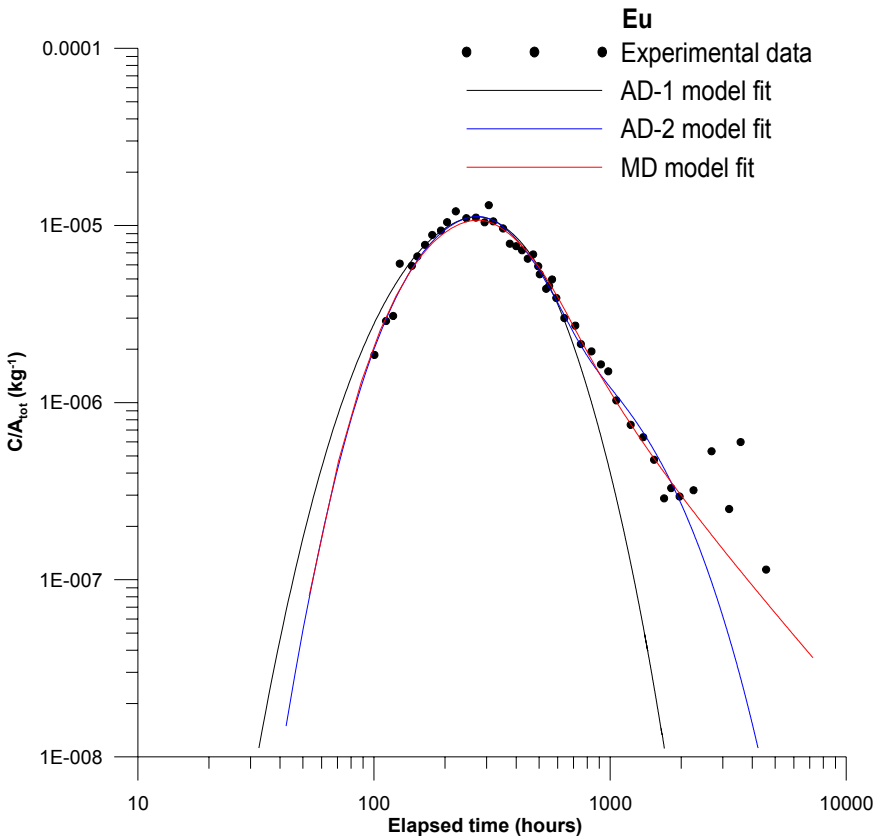

***Figure 4-2b**. Logarithmic plot of model fits for ^{155}Eu-DTPA.*

The model fitting of the non-sorbing tracers indicates that both the AD-2 model and the MD model give fairly good agreement between model and experimental data, while less good agreement is obtained using the AD-1 model. The discrepancy between data and the AD-1 model is primarily apparent in the tail parts. Of the AD-2 and MD model fits, it may be argued that the MD model fit is to be preferred because of lower estimation errors, fewer parameters and slightly better fit at the end of the curves in the log-log plots.

The parameter values obtained using the MD model for the HTO and ^{155}Eu-DTPA breakthrough curves, respectively, differ slightly. The HTO curve results in somewhat shorter residence time and larger matrix diffusion effect than for ^{155}Eu-DTPA. Of these two tracers, ^{155}Eu-DTPA was chosen as a non-sorbing tracer for further analysis of the sorbing tracers. The main reasons for this choice are the un-explained low recovery of HTO and that ^{155}Eu-DTPA is measured using the method as is used for the sorbing tracers.

Sorbing tracers

The sorbing tracers were evaluated by simultaneous model fitting of non-sorbing and sorbing tracers using the MD model (advection-dispersion with matrix diffusion). As indicated by the discussion in the preceding section, ^{155}Eu-DTPA was chosen as the non-sorbing tracer to be used for evaluation of sorbing tracers.

First, each sorbing tracer was evaluated individually. Thus, one estimation run was carried out for each pairing of ^{155}Eu-DTPA and a sorbing tracer. The results for these runs are presented in Table 4-2. There were 7 estimation parameters for each such pair. Two of the parameters, t_0 (residence time) and a_L, are common to both tracers. The parameters *pf* (proportionality factor) and *A* (matrix diffusion parameter) are estimated for each tracer, while *R* (retardation factor) is estimated for the sorbing tracer. The model fits for these cases are shown in Figures 4-3a-c.

In addition, two estimation runs with multiple tracers were carried out: one with ^{155}Eu-DTPA, $^{22}Na^{+}$, $^{133}Ba^{2+}$ and one with all sorbing tracers (^{155}Eu-DTPA, $^{22}Na^{+}$,; $^{133}Ba^{2+}$, $^{54}Mn^{2+}$). These results are presented in Table 4-3 and in Figures 4-4 and 4-5.

Table 4-2. Parameter estimation results for sorbing tracers (pair-wise) for flow path KI0025F02:R2 - KI0025F03:R3 (slow flow path). Estimation errors expressed as coefficient of variation are given within parentheses.

		^{155}Eu-DTPA – $^{22}Na^{+}$		^{155}Eu-DTPA – $^{133}Ba^{2+}$		^{155}Eu-DTPA - $^{54}Mn^{2+}$	
Parameter	**Units**	**Eu**	**Na**	**Eu**	**Ba**	**Eu**	**Mn**
t_0	h	217 (0.12)	-	223 (0.18)	-	208 (0.17)	-
a_L	m	2.5 (0.17)	-	2.4 (0.36)	-	3.5 (0.28)	-
Pf	-	$7.7\cdot10^{-4}$ (0.09)	$6.2\cdot10^{-4}$ (0.03)	$7.9\cdot10^{-4}$ (0.07)	$3.7\cdot10^{-4}$ (0.17)	$7.9\cdot10^{-4}$ (0.04)	$2.5\cdot10^{-4}$ (1.58)
R	-	-	1.5 (0.11)	-	4.5 (0.36)	-	7.4 (2.17)
A	$s^{½}$	1612 (0.40)	730 (0.19)	1548 (0.45)	389 (0.49)	1232 (0.34)	276 (2.86)

Table 4-3. Parameter estimation results for sorbing tracers (multiple tracers) for flow path KI0025F02:R2 - KI0025F03:R3 (slow flow path). Estimation errors expressed as coefficient of variation are given within parentheses.

		^{155}Eu-DTPA – $^{22}Na^{+}$ - $^{133}Ba^{2+}$			^{155}Eu-DTPA – $^{22}Na^{+}$ – $^{133}Ba^{2+}$ – $^{54}Mn^{2+}$			
Parameter	**Units**	**Eu**	**Na**	**Ba**	**Eu**	**Na**	**Ba**	**Mn**
t_0	h	218 (0.12)	-	-	217 (0.12)	-	-	-
a_L	m	2.2 (0.19)	-	-	2.4 (0.19)	-	-	-
Pf	-	$7.6\cdot10^{-4}$ (0.08)	$6.5\cdot10^{-4}$ (0.02)	$5.5\cdot10^{-4}$ (0.26)	$7.7\cdot10^{-4}$ (0.08)	$6.6\cdot10^{-4}$ (0.02)	$4.8\cdot10^{-4}$ (0.23)	$2.3\cdot10^{-4}$ (3.71)
R	-	-	1.3 (0.11)	4.1 (0.45)	-	1.4(0.11)	4.1 (0.42)	6.4 (4.43)
A	$s^{½}$	1636 (0.39)	587 (0.20)	302 (0.57)	1490 (0.37)	607 (0.20)	307 (0.54)	291 (5.98)

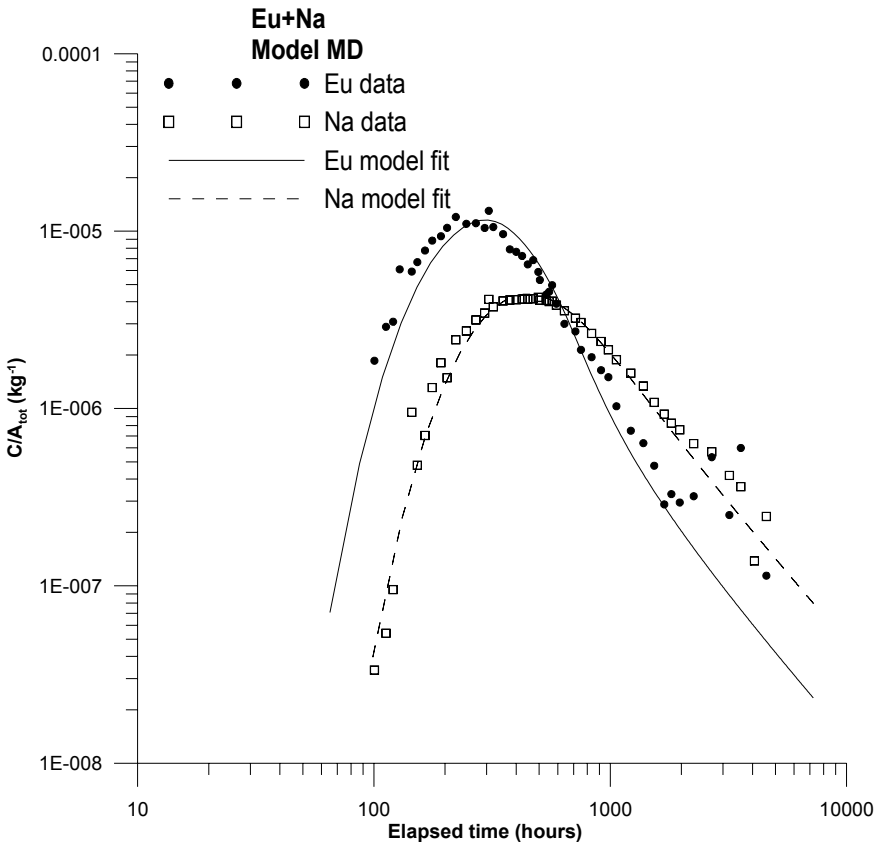

***Figure 4-3a**. Logarithmic plot of results from simultaneous fitting of ^{155}Eu-DTPA and $^{22}Na^{+}$.*

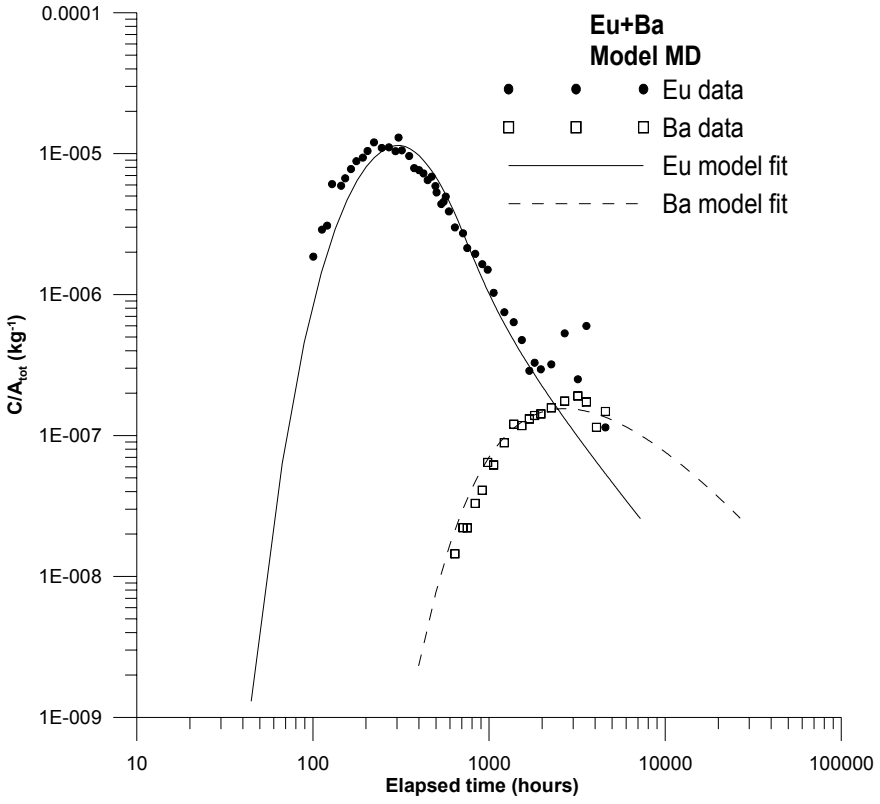

***Figure 4-3b**. Logarithmic plot of results from simultaneous fitting of ^{155}Eu-DTPA and $^{133}Ba^{2+}$.*

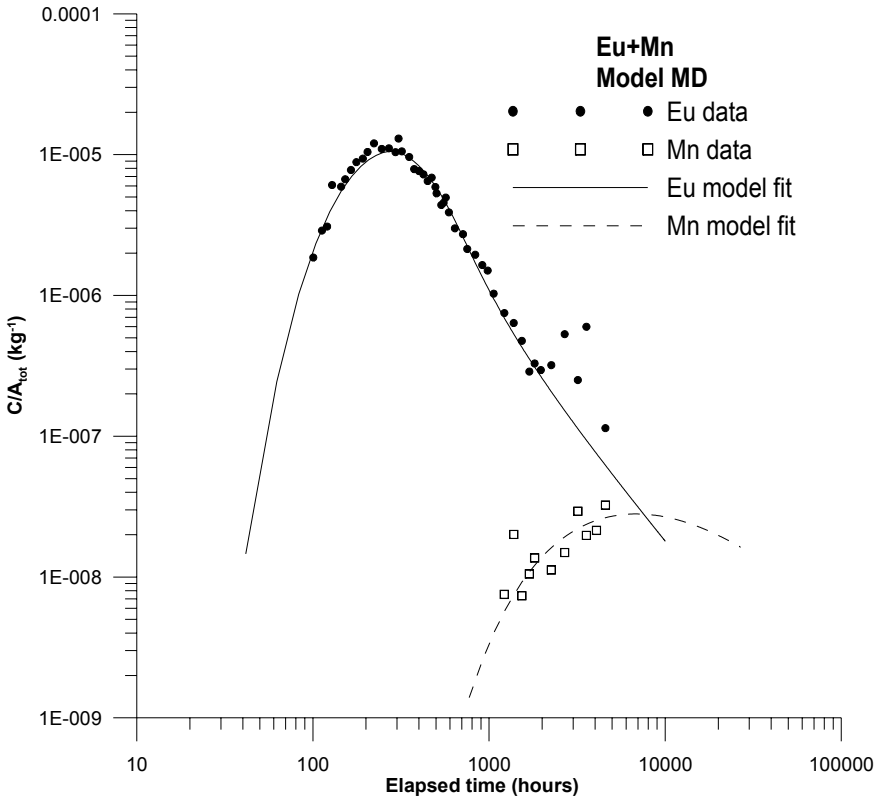

***Figure 4-3c**. Logarithmic plot of results from simultaneous fitting of ^{155}Eu-DTPA and $^{54}Mn^{2+}$.*

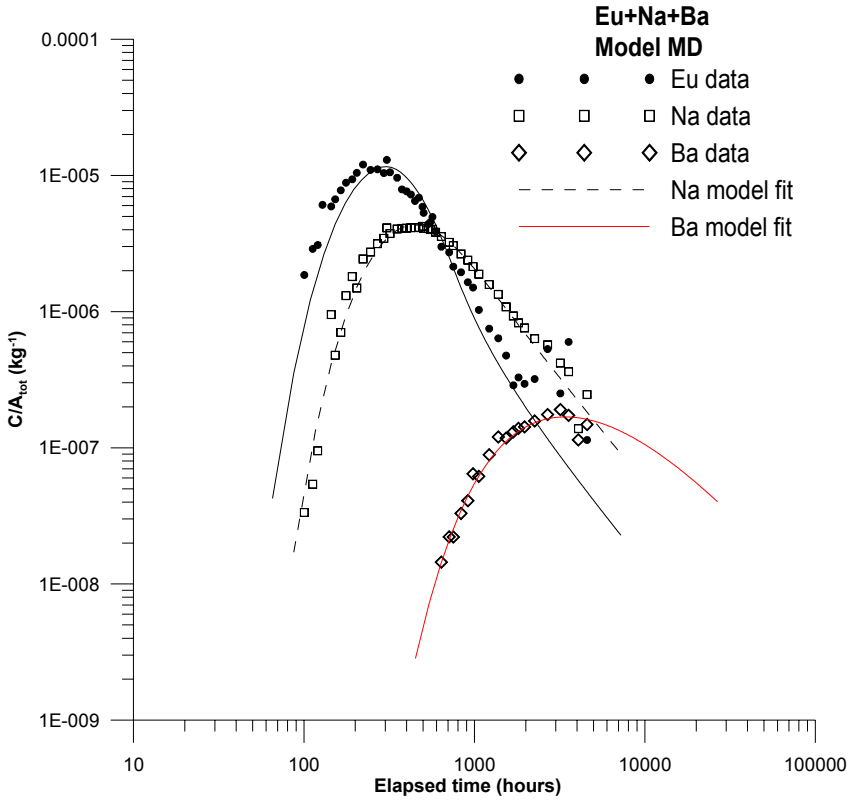

***Figure 4-4**. Logarithmic plot of results from simultaneous fitting of ^{155}Eu-DTPA, $^{22}Na^{+}$ and $^{133}Ba^{2+}$.*

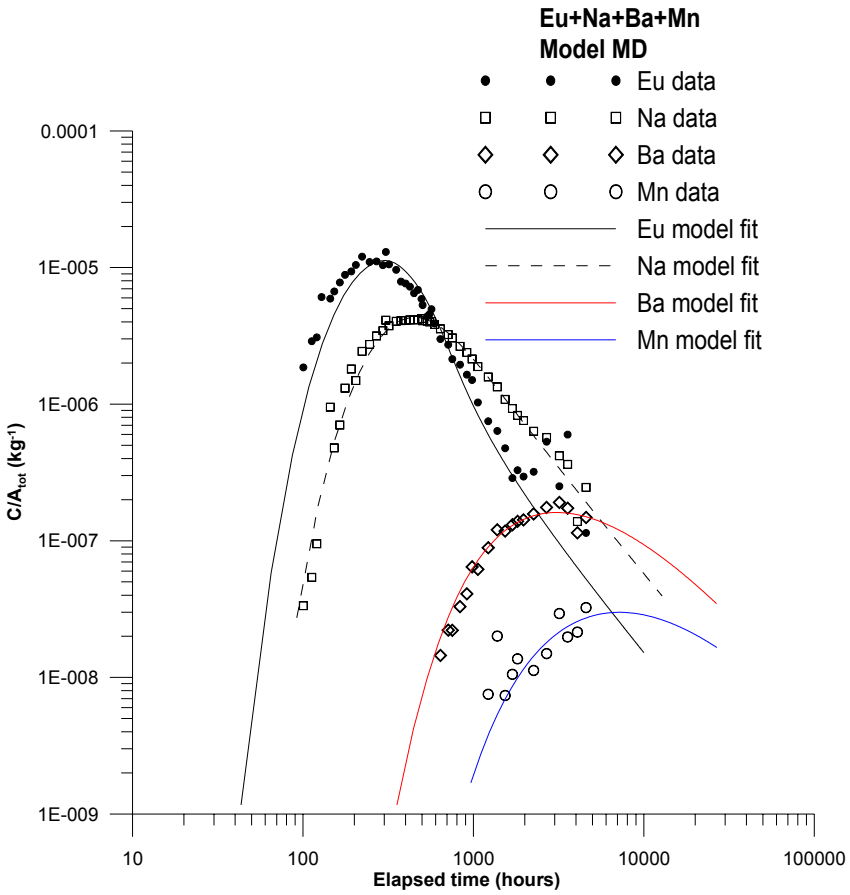

***Figure 4-5**. Logarithmic plot of results from simultaneous fitting of ^{155}Eu-DTPA, $^{22}Na^{+}$, $^{133}Ba^{2+}$ and $^{54}Mn^{2+}$.*

In all of the plots above, involving sorbing tracers, there is relatively good agreement between model and experimental data. The breakthrough curve for $^{54}Mn^{2+}$ only has data for the rising part, and thus, estimation is very uncertain in these cases. This is clearly reflected in the estimation statistics showing very large CV (coefficient of variation) for all estimates related to $^{54}Mn^{2+}$. An examination of the correlation matrix (not shown) also shows that that several parameter pairs are highly correlated. For the other sorbing tracers ($^{22}Na^{+}$ and $^{133}Ba^{2+}$), estimation statistics indicate a more well-defined model fit. The retardation factors for these tracers are estimated to about 1.3 - 1.5 for $^{22}Na^{+}$ and about 4.1 - 4.5 for $^{133}Ba^{2+}$. There is also an increasing matrix diffusion effect such that Eu<Na<Ba.

4.6.3 Flow path KI0025F02:R3 - KI0025F03:R3

Non-sorbing tracers

Non-sorbing tracers for this flow path were $^{131}I^{-}$ and ^{160}Tb-DTPA. Both of these tracers were analysed using the AD (advection-dispersion; see section 4.2) and MD (advection-dispersion with matrix diffusion; see Section 4.2) models. The results are summarised in Table 4-4 and the model fits are shown in Figures 4-6 and 4-7 for $^{131}I^{-}$ and ^{160}Tb-DTPA, respectively.

Table 4-4. Parameter estimation results for non-sorbing tracers for flow path KI0025F02:R3 - KI0025F03:R3 (fast flow path). Estimation errors expressed as coefficient of variation are given within parentheses.

Model	Parameter	Units	$^{131}I^-$		^{160}Tb-DTPA	
AD-1	t_0	h	13.4	(0.04)	19.4	(0.05)
	a_L	m	7.9	(0.12)	8.8	(0.10)
	pf		$1.4 \cdot 10^{-3}$	(0.03)	$1.7 \cdot 10^{-3}$	(0.06)
AD-2	$t_{0,1}$	h	11.0	(0.11)	13.1	(0.06)
	$a_{L,1}$	m	2.7	(0.11)	4.2	(0.07)
	pf_1		$1.1 \cdot 10^{-3}$	(0.44)	$1.3 \cdot 10^{-3}$	(0.16)
	$t_{0,2}$	h	60	(1.30)	77	(1.12)
	$a_{L,2}$	m	15	(3.36)	22	(2.52)
	pf_2		$4.9 \cdot 10^{-5}$	(0.78)	$3.8 \cdot 10^{-4}$	(0.53)
MD	t_0	H	6.3	(0.12)	7.6	(0.08)
	a_L	M	1.0	(0.24)	1.5	(0.14)
	pf		$1.8 \cdot 10^{-3}$	(0.03)	$1.8 \cdot 10^{-3}$	(0.02)
	A	$S^{½}$	119	(0.17)	166	(0.11)

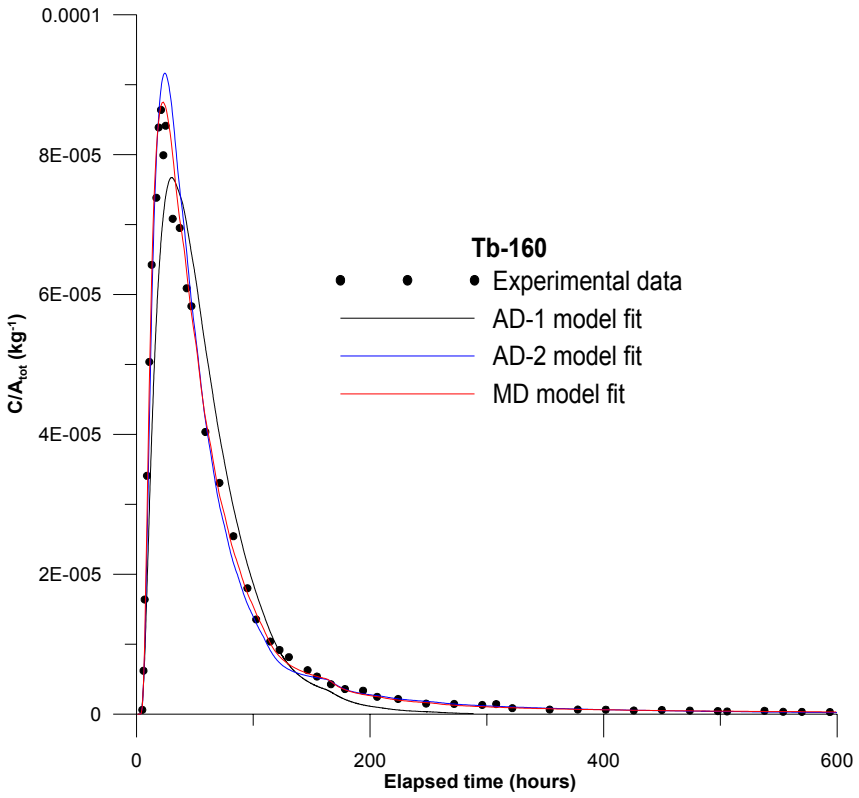

***Figure 4-6a**. Linear plot of model fits for ^{160}Tb-DTPA.*

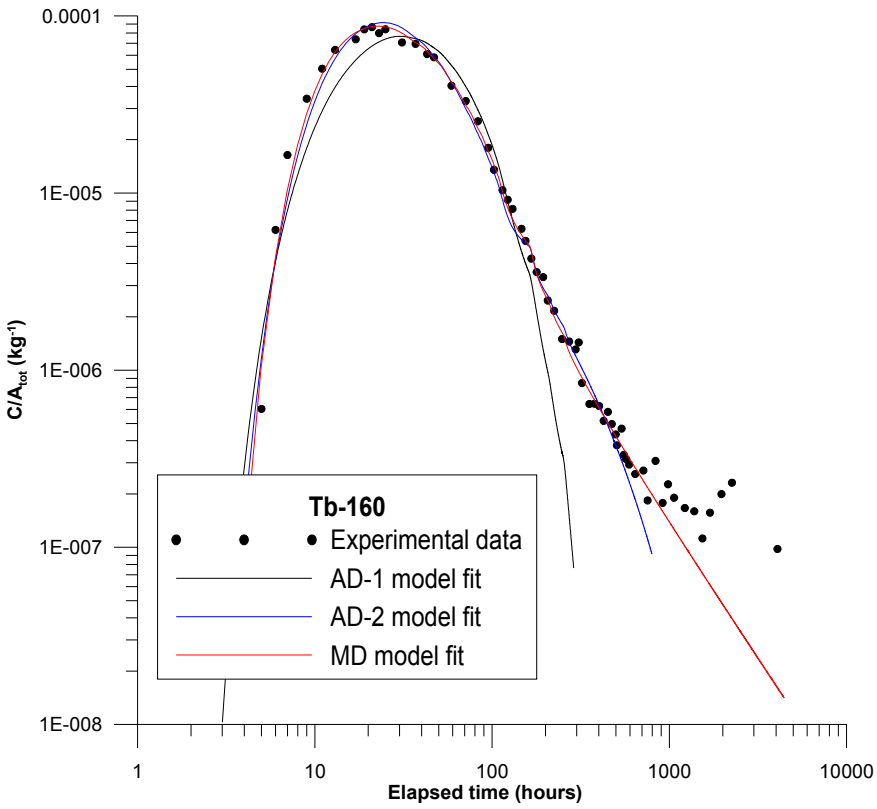

***Figure 4-6b**. Logarithmic plot of model fits for ^{160}Tb-DTPA.*

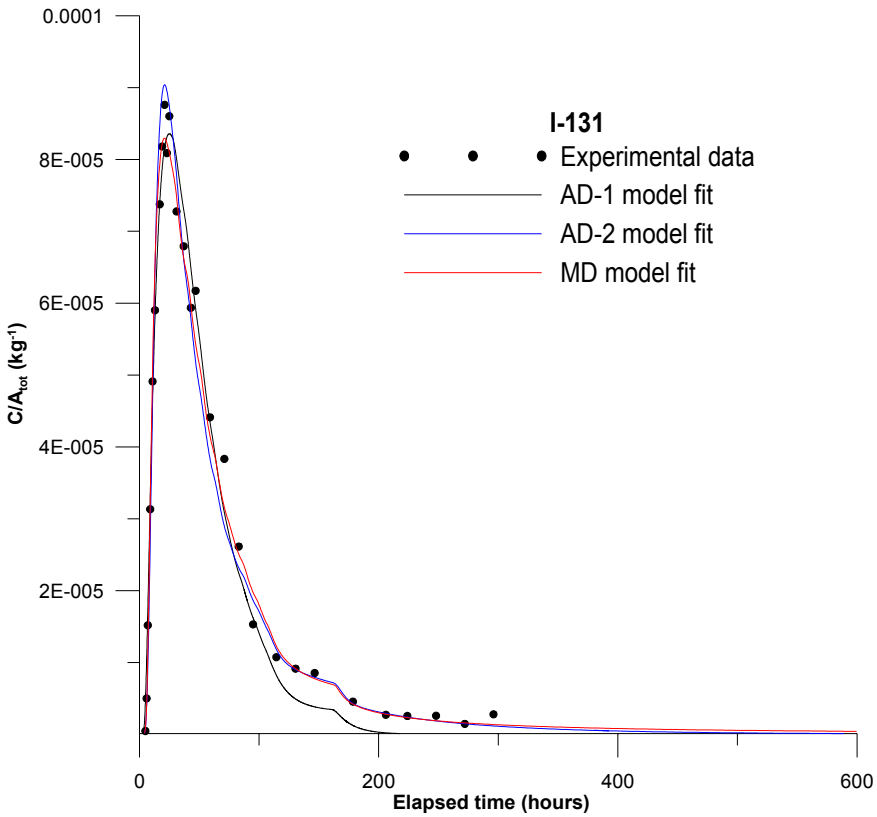

***Figure 4-7a**. Linear plot of model fits for ^{131}I.*

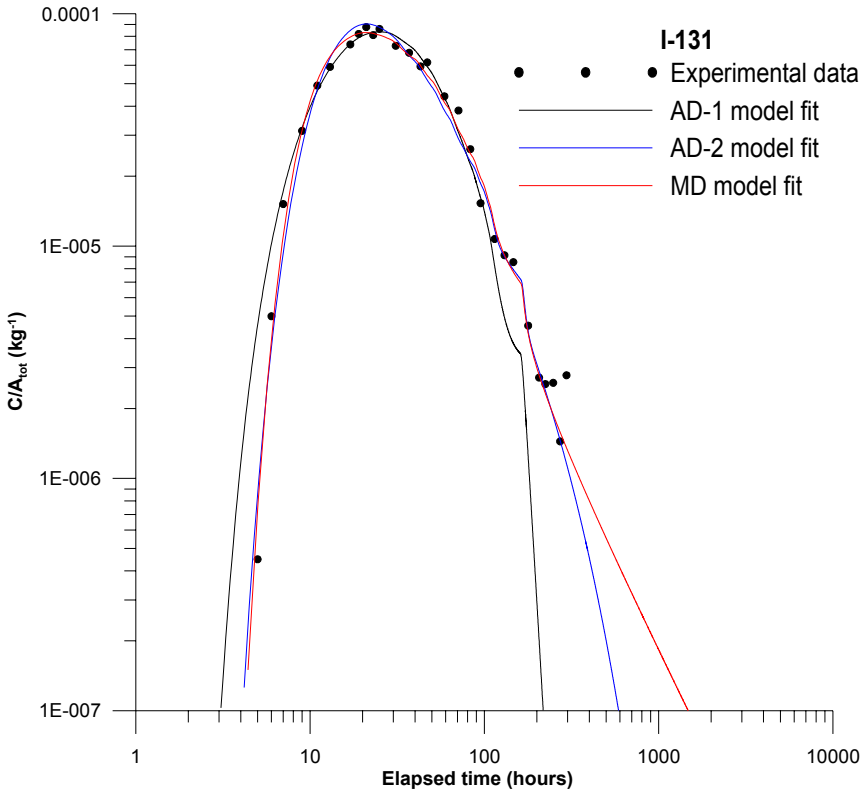

***Figure 4-7b**. Logarithmic plot of model fits for $^{131}I^-$.*

The model fitting of the non-sorbing tracers indicates that both the AD-2 model and the MD model give fairly good agreement between model and experimental data, while less good agreement is obtained using the AD-1 model. As was seen for the slower flow path evaluated above, the discrepancy between data and the AD-1 model is primarily apparent in the tail parts. Of the AD-2 and MD model fits, it may be argued that the MD model fit is to be preferred because of lower estimation errors, fewer parameters and slightly better fit at the end of the curves in the log-log plots.

The parameter values obtained using the MD model for the $^{131}I^-$ and ^{160}Tb-DTPA breakthrough curves, respectively, differ slightly, despite the close agreement between the experimental breakthrough curves for these tracers. The differences in estimated parameter values are likely an effect of the high sensitivity of the model fitting to the tracer injection data. Because the transport is so fast relative to the duration of tracer injection, small errors in tracer injection input data may give different parameter estimates. This is different than for the slower path, where the sensitivity to the tracer injection function is much smaller.

Some of the differences between $^{131}I^-$ and ^{160}Tb-DTPA may also be attributed to the fact that more data (longer times) are available for ^{160}Tb-DTPA than for $^{131}I^-$. For this reason, ^{160}Tb-DTPA is also chosen as the non-sorbing tracer for further analysis of the sorbing tracers.

Sorbing tracers

The sorbing tracers were evaluated by simultaneous model fitting of non-sorbing and sorbing tracers using the MD model (advection-dispersion with matrix diffusion and equilibrium sorption). As indicated by the discussion in the preceding section, ^{160}Tb-DTPA was chosen as the non-sorbing tracer to be used for evaluation of sorbing tracers.

First, each sorbing tracer was evaluated individually. Thus, one estimation run was carried out for each pairing of ^{160}Tb-DTPA and a sorbing tracer. The results for these runs are presented in Table 4-5. There were 7 estimation parameters for each such pair. Two of the parameters, t_0 (residence time) and *Pe* (Peclet number), are common to both tracers. The parameters *pf* (proportionality factor) and *A* (matrix diffusion parameter) are estimated for each tracer, while *R* (retardation factor) is estimated for the sorbing tracer. The model fits for these cases are shown in Figures 4-8 a-c.

In addition, two estimation runs with multiple tracers were carried out: one with ^{160}Tb-DTPA, $^{85}Sr^{2+}$, $^{86}Rb^{+}$ and one with all of the sorbing tracers (^{160}Tb-DTPA, $^{85}Sr^{2+}$, $^{86}Rb^{+}$, $^{137}Cs^{+}$). These results are presented in Table 4-6 and in Figures 4-9 and 4-10.

Table 4-5. Parameter estimation results for sorbing tracers (pairwise) for flow path KI0025F02:R3 - KI0025F03:R3 (fast flow path). Estimation errors expressed as coefficient of variation are given within parentheses.

		^{160}Tb-DTPA – $^{85}Sr^{2+}$		^{160}Tb-DTPA – $^{86}Rb^{+}$		^{160}Tb-DTPA – $^{137}Cs^{+}$	
Parameter	**Units**	**Tb**	**Sr**	**Tb**	**Rb**	**Tb**	**Cs**
t_0	h	10.9 (0.11)	-	11.3 (0.07)	-	10.0 (0.09)	-
a_L	m	2.5 (0.17)	-	2.8 (0.11)	-	2.4 (0.14)	-
pf	-	$1.9\cdot10^{-3}$ (0.03)	$1.9\cdot10^{-3}$ (0.03)	$1.8\cdot10^{-3}$ (0.02)	$1.1\cdot10^{-3}$ (0.17)	$1.8\cdot10^{-3}$ (0.02)	$1.1\cdot10^{-3}$ (0.05)
R	-	-	1.13 (0.06)	-	3.24 (0.47)	-	13.2 (0.19)
A	$s^{½}$	274 (0.17)	132 (0.17)	286 (0.11)	166 (0.71)	227 (0.13)	136 (0.27)

Table 4-6. Parameter estimation results for sorbing tracers (multiple tracers) for flow path KI0025F02:R3 - KI0025F03:R3 (fast flow path). Estimation errors expressed as coefficient of variation are given within parentheses.

		^{160}Tb-DTPA - $^{85}Sr^{2+}$ - $^{86}Rb^{+}$			^{160}Tb-DTPA - $^{85}Sr^{2+}$ - $^{86}Rb^{+}$ - $^{137}Cs^{+}$			
Parameter	**Units**	**Tb**	**Sr**	**Rb**	**Tb**	**Sr**	**Rb**	**Cs**
t_0	h	12.6 (0.11)	-	-	12.1 (0.09)	-	-	-
a_L	m	3.3 (0.16)	-	-	3.0 (0.14)	-	-	-
pf	-	$1.9\cdot10^{-3}$ (0.03)	$2.0\cdot10^{-3}$ (0.03)	$1.2\cdot10^{-3}$ (0.29)	$1.9\cdot10^{-3}$ (0.02)	$1.9\cdot10^{-3}$ (0.02)	$1.3\cdot10^{-3}$ (0.25)	$1.1\cdot10^{-3}$ (0.08)
R	-	-	1.24 (0.05)	3.01 (0.81)	-	1.20 (0.05)	2.90 (0.80)	12.8 (0.20)
A	$s^{½}$	316 (0.16)	181 (0.16)	150 (1.21)	321 (0.15)	165 (0.14)	132 (1.13)	162 (0.29)

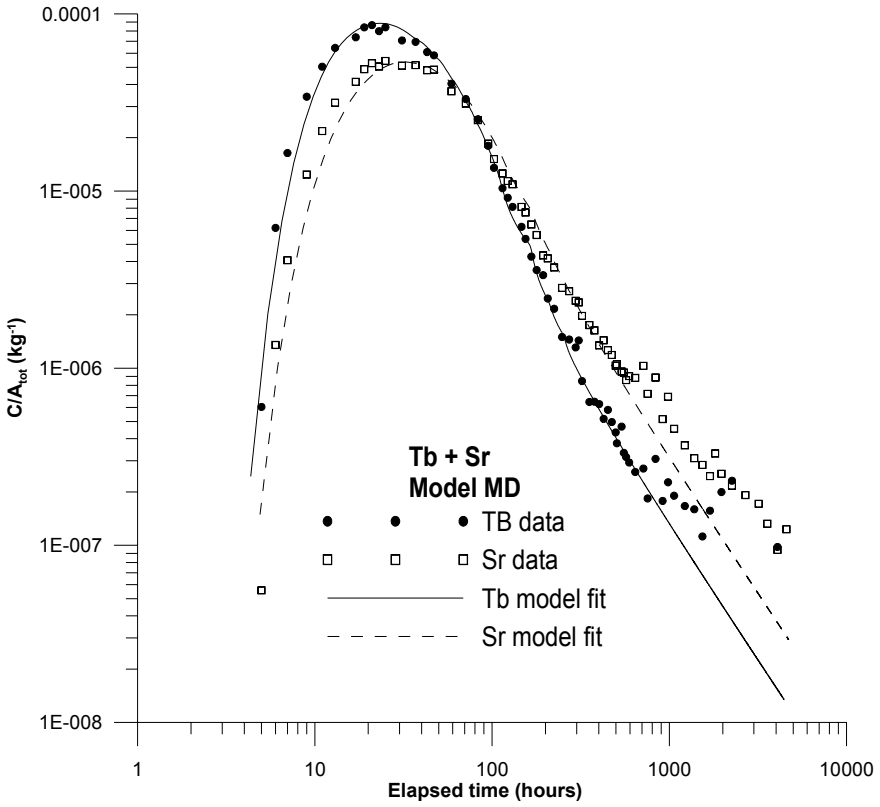

***Figure 4-8a**. Logarithmic plot of results from simultaneous fitting of ^{160}Tb-DTPA and $^{85}Sr^{2+}$.*

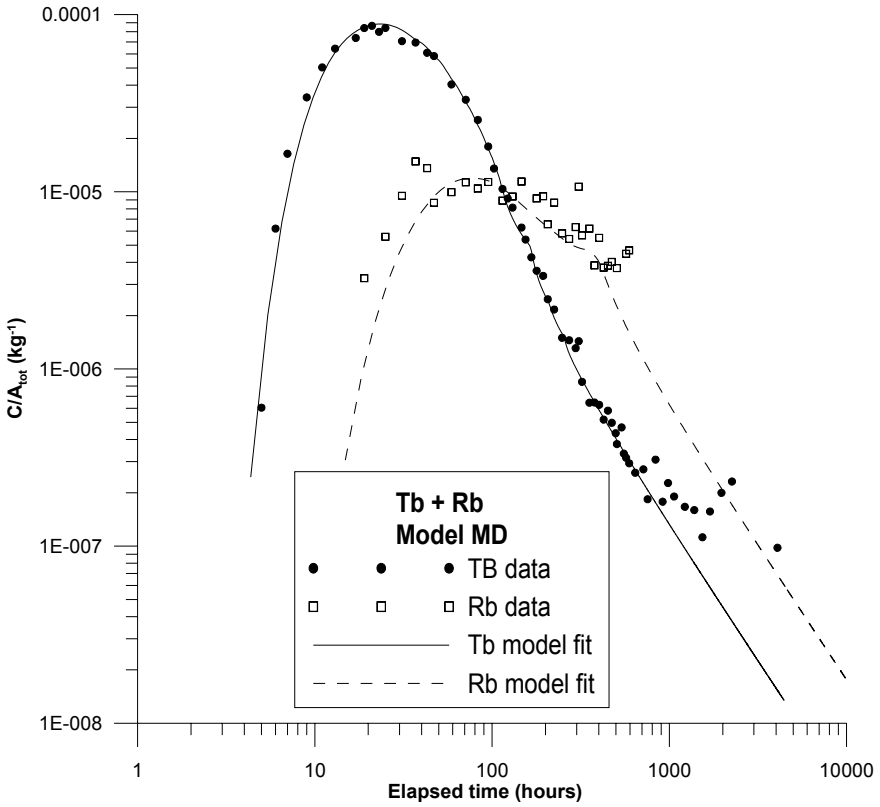

***Figure 4-8b**. Logarithmic plot of results from simultaneous fitting of ^{160}Tb-DTPA and $^{86}Rb^{+}$.*

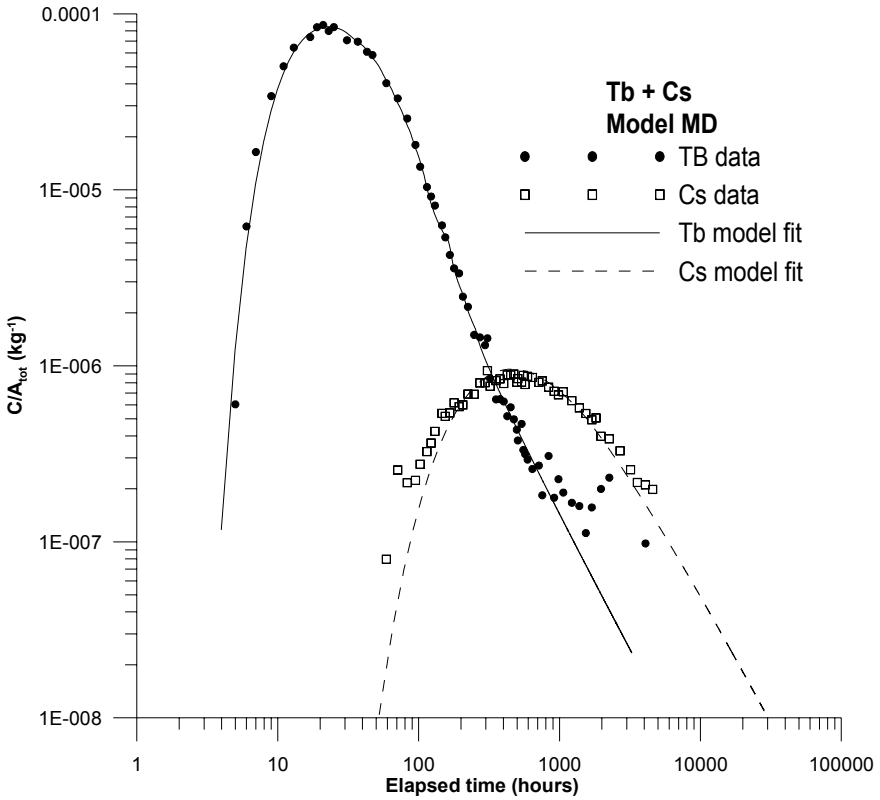

***Figure 4-8c**. Logarithmic plot of results from simultaneous fitting of ^{160}Tb-DTPA and $^{137}Cs^{+}$.*

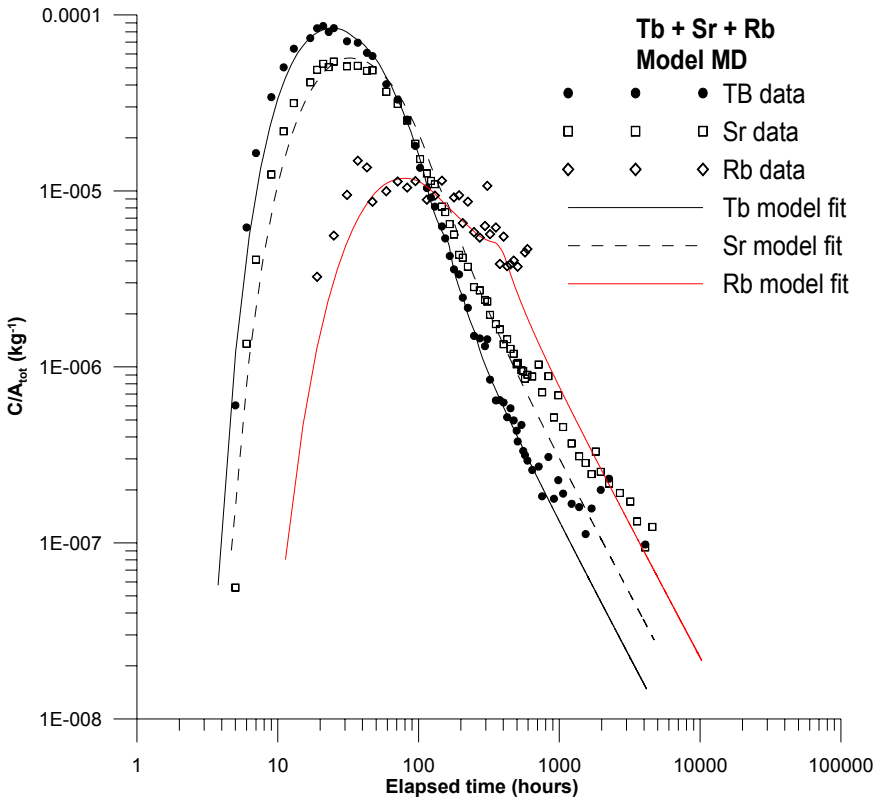

***Figure 4-9**. Logarithmic plot of results from simultaneous fitting of ^{160}Tb-DTPA, $^{85}Sr^{2+}$ and $^{86}Rb^{+}$.*

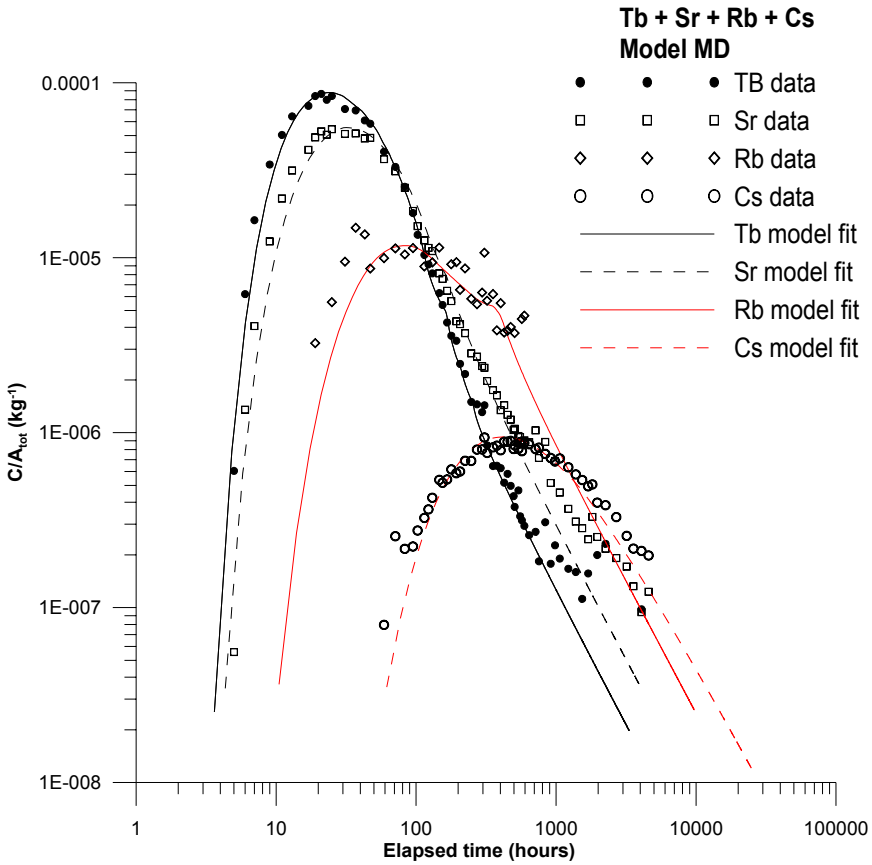

***Figure 4-10**. Logarithmic plot of results from simultaneous fitting of ^{160}Tb-DTPA, $^{85}Sr^{2+}$, $^{86}Rb^{+}$ and $^{137}Cs^{+}$.*

In all of the plots above, involving sorbing tracers, there is relatively good agreement between model and experimental data. The breakthrough curve for $^{86}Rb^{+}$ only contains somewhat noisy data around the peak, and thus, estimated parameters related to $^{86}Rb^{+}$ have relatively large estimation errors. For the other sorbing tracers ($^{85}Sr^{2+}$ and $^{137}Cs^{+}$), estimation statistics indicate a more well-defined model fit. The retardation factors for these tracers are estimated to about 1.1 - 1.25 for $^{85}Sr^{2+}$ and about 12.8 - 13.2 for $^{137}Cs^{+}$. The matrix diffusion effect, as indicated by the parameter *A,* is relatively high for all tracers. There is also a tendency to an increasing matrix effect with increasing sorption capacity.

Based on estimates of t_0 (tracer residence time), the equivalent fracture conductivity (eq. 4-11) and the equivalent fracture aperture (eq. 4-12) may be estimated. Such estimates are based on simplifying assumptions of homogenous radial flow, and may in this case be regarded as meaningful only for the faster of the flow paths. Based on t_0 estimates for ^{160}Tb-DTPA (the case with simultaneous estimation using four tracers), K_{fr} is 1.4 x 10^{-4} m/s and δ is 1.5 x 10^{-3} m for the faster flow path. These values are based on t_0 = 12.1 h, r = 19.5 m, r_w = 0.038 m, Q_{bh} = 4.17 x 10^{-5} m^3/s, and Δh = 200 m.

4.6.4 Theoretical tracer recovery

The theoretical tracer recovery, calculated according to eq. 4-18, for the two cases where four tracers were estimated simultaneously (Tables 4-3 and 4-6, respectively) is shown in Table 4-7. The calculated recovery values agree approximately with the values in Tables 3-3 and 3-4 (based on experimental data). The model recovery for ^{155}Eu-DTPA is lower than in Table 3-4, probably because the fitted curve does not include some of the high concentrations around the peak. The model recovery values for the sorbing tracers are generally higher than the corresponding values in Tables 3-3 and 3-4 because the model curve extends the experimental curves beyond the last sampling occasion. Thus, these values may be considered to represent a "maximum" plausible value for these tracers. Nevertheless, it is apparent that the recovery for $^{133}Ba^{2+}$, $^{54}Mn^{2+}$ and $^{137}Cs^{+}$ is significantly lower than for the other tracers.

Table 4-7. Theoretical tracer recovery calculated from simultaneous estimation of ^{155}Eu-DTPA, $^{22}Na^{+}$, $^{133}Ba^{2+}$, $^{54}Mn^{2+}$ (slow flow path) and ^{160}Tb-DTPA, $^{85}Sr^{2+}$, $^{86}Rb^{+}$, $^{137}Cs^{+}$ (fast flow path), respectively.

Tracer	Recovery (%)
^{155}Eu-DTPA	83.2
$^{22}Na^{+}$	83.1
$^{133}Ba^{2+}$	31.9
$^{54}Mn^{2+}$	8.9
^{160}Tb-DTPA	85.9
$^{85}Sr^{2+}$	85.4
$^{86}Rb^{+}$	75.1
$^{137}Cs^{+}$	37.3

5 Discussion and conclusions

5.1 Equipment and procedures

The TRUE Block Scale Continuation BS2B tracer tests were performed using techniques and equipment earlier developed and used in the TRUE Block Scale Phase C experiments (Andersson et al., 2001). In general, the procedures and equipment worked well with only a few minor problems. The only problem that to some degree influences the results is the clogged filter in the circulation loop of KI0025F02:R2, injection section in the slow flow path (BG#1). The resulting poor mixing, especially during the first hours of injection, gives a somewhat uneven tracer distribution. However, the on-line measurement of the input activity makes it possible to take this into account in the evaluation.

5.2 Transport properties

The evaluation of the breakthrough data was performed with the same models and concepts as previous tests with sorbing tracers in the TRUE Block Scale, Phase C tests (Andersson et al., 2001). The following main results were obtained:

- Experimental data fits relatively well to a one-dimensional advection-dispersion model with matrix diffusion and linear equilibrium sorption. The fit to the models without matrix diffusion is generally less good.
- The following approximate value ranges for R (retardation coefficient) for the sorbing tracers were found (in rising order):
- $^{85}Sr^{2+}$: 1.1 – 1.25
- $^{22}Na^{+}$: 1.3 – 1.5
- $^{86}Rb^{+}$: 2.9 – 3.2
- $^{133}Ba^{2+}$: 4.1 – 4.5
- $^{54}Mn^{2+}$: 6.4 – 7.4
- $^{137}Cs^{+}$: 12.8 – 13.2
- The values for $^{54}Mn^{2+}$ are associated with large estimation errors. This is also the case, but to a lesser extent, for $^{86}Rb^{+}$.
- The matrix diffusion effect is probably fairly significant in both of the tested flow paths, based on estimated values of parameter A. Further evaluation of A (i.e. to determine D_e) requires estimates of the fracture aperture and the matrix porosity (eq. 4-10). Lower values of A for non-sorbing tracers were found in the faster of the flow paths but, again, the significance of this depends on the values of the aperture and matrix porosity in each flow path.

- Estimated dispersivity values (generally about 2 – 3 m) were on the order of one magnitude smaller than the Euclidian transport distance.

- Estimated residence times were about 10 – 12 hours for the faster flow path, and about 200 – 220 hours for the slower flow path.

- The evaluation of the faster flow path was found to be very sensitive to the injection input function. An accurate description of the injection function was possible by using the on-line measurements at early stages of the injection.

- Theoretical tracer recovery relatively good for most of the tracers (75-85 %). Significantly lower theoretical recovery was found for three of the sorbing tracers: $^{137}Cs^{+}$ (37 %), $^{133}Ba^{2+}$ (32 %) and $^{54}Mn^{2+}$ (9 %).

The results of the modelling show both similarities and differences when compared to the TRUE Block Scale Phase C tests (Andersson et al., 2001). The main difference is that $^{85}Sr^{2+}$ shows a significantly lower retardation than in the Phase C tests, in fact also lower than for $^{22}Na^{+}$. The flow paths are also significantly different. Phase C (injection C3) was performed in a long and slow flow path (t_0 =820 h) whereas in this case in a fast flow path (Structure #19, t_0=10 h).

6 References

Andersson, P., Gröhn, S., Nordqvist, R., Wass, E., 2004: TRUE Block Scale Continuation, BS2 Pretests. Crosshole interference, dilution and tracer tests, CPT-1 - CPT- 4. SKB International Progress Report IPR-04-25.

Andersson, P., Byegård, J., Dershowitz, B., Doe, T., Hermansson, J., Meier, P., Tullborg, E.-L.,Winberg, A., 2002a: Final report of the TRUE Block Scale project 1. Characterisation and model development. SKB Technical Report TR-02-13.

Andersson, P., Byegård, J., Winberg, A., 2002b: Final report of the TRUE Block Scale project. 2. Tracer tests in the block scale. SKB Technical Report TR-02-14.

Andersson, P., Byegård, J., Holmqvist, M., Skålberg, M., Wass, E., Widestrand, H., 2001: TRUE Block Scale Project. Tracer tests stage. Tracer tests, Phase C. SKB International Progress Report IPR-04-25.

Andersson, P., Wass, E., Holmqvist, M., **Fierz, T., 2000:** TRUE Block Scale Project Tracer Tests Stage. Tracer tests, Phase B. SKB International Progress Report IPR-00-29.

Andersson, P., 1996: TRUE 1st stage Tracer Test Programme. Experimental data preliminary evaluation of the TRUE-1 radially converging tracer test (RC1). SKB International Progress Report HRL-96-24.

Byegård, J., 2002: Tracer Retention Understanding Experiments. Continued sampling and tracer measurements in the TRUE-1 experiment and TRUE Block Scale experiment, Phase C. SKB International Progress Report IPR-02-69.

Byegård, J., Skarnemark, G., Skålberg, M., 2000: Transport modelling of tracers influenced by kinetic hindered sorption – applied to laboratory and in situ studies of lanthanide EDTA complexes. Journal of Contaminant Hydrology 42 (2000), 165-186.

Byegård, J., Johansson, H., Skålberg, M., Tullborg, E-L., 1998: The interaction of sorbing and non-sorbing tracers with different Äspö rock types. SKB Technical Report TR-98-18.

Cooley, R., L., 1979: A method of estimating parameters and assessing reliability for models of steady state ground water flow. 2. Application of statistical analysis. Water Resources Research, 13: 603-617.

Dershowitz, W., Winberg, A., Hermanson, J., Byegård, J., Tullborg, E-L., Andersson, P., Mazurek, M., 2003: Äspö Task Force on modelling of groundwater flow and transport of solutes. Task 6C, A semi-synthetic model of block scale conductive structures at the Äspö HRL. SKB International Progress Report IPR-03-13.

Holmqvist, M., Byegård, J., Fierz, T., Trick, T., Eichinger, L., Scholits, A., 2002: Tests of new possible non-reactive tracers – experimental description and evaluation. SKB International Progress Report IPR-02-71.

Ittner, T., Byegård, J., 1997: Test of tracer sorption on equipment. SKB International Progress Report HRL-97-28.

Javandel, I., Doughty, C., Tsang, C. F., 1984: Groundwater transport: Handbook of mathematical models. American Geophysical Union, Water resources monograph series 10.

Levenberg, K., 1944: A method for the solution of certain nonlinear problems in least squares. Q. Appl. Math., 2: 164-168.

Marquardt, D., W., 1963: An algorithm for least squares estimation of non-linear parameters. J. Soc. Ind. Appl. Math. 11: 431-441.

Moreno, L., Neretnieks, I., Klockars, C-E, 1983: Evaluation of some tracer tests in the granitic rock at Finnsjön. SKBF/KBS Technical Report 83-38.

Moreno, L., Neretnieks, I., Eriksen, T., 1985: Analysis of some laboratory runs in natural fissures. Water Resources Research 21(7): 951-958.

Nordqvist, R., 1994: Documentation of some analytical flow and transport models implemented for use with PAREST - Users manual. GEOSIGMA Internal Report GRAP 94 006, Uppsala.

Poteri, A., Billaux, D., Dershowitz, W., Gomez-Hernandez, J J., Cvetkovic, V., Hautojärvi, A., Holton, D., Medina, A., Winberg, A., 2002: Final report of the TRUE Block Scale project. 3. Modelling of flow and transport. SKB Technical Report TR-02-15.

Tang, D.H., Frind, E.O., Sudicky E.A., 1981: Contaminant transport in fractured porous media: analytical solution for a single fracture. Water Resources Research 17(3): 555-564.

Winberg, A., Andersson, P., Poteri, A., Cvetkovic, V.Dershowitz, W., Hermanson, J., Gomez-Hernandez, J J., Hautojärvi, A., Billaux, D., Tullborg, E-L., Holton, D., Meier, P., Medina, A., 2002: Final report of the TRUE Block Scale project. 4. Synthesis of flow, transport and retention in the block scale. SKB Technical Report TR-02-16.

Winberg, A., Andersson, P., Hermanson, J., Byegård, J., Cvetkovic, V., Birgersson, L., 2000 : Äspö Hard Rock Laboratory, Final report of the first stage of the tracer retention understanding experiments, SKB Technical report TR-00-07.

Winberg, A., 1997: Test plan for the TRUE Block Scale Experiment. SKB International Cooperation Report ICR 97-02.

Appendix 1 Packer positions in boreholes KI0025F02 and KI0025F03 before and after re-instrumentation in September 2003.

Instrumentation of KI0025F03

Instrumentation was focused on Structure #19 at 125 m and ”background fracture BG#2” close to #19 at 133 m. Sections P5 and P7 (in yellow) were left “untouched” due to radioactive contamination from previous tracer tests.

OLD				NEW		
Borehole/section	Borehole Length		Struct	Borehole/section	Borehole Length	Structure
25F03P1	101.0-141.7		10, 25, 19	25F03R1	135.03-141.72	10
25F03P2	93.5-100.0		?	25F03R2	129.03-134.03	25
25F03P3	89.0-92.5	C	13	25F03R3	123.03-128.03	19
25F03P4	85.0-88.0	C	21	25F03R4	93.53-122.03	?
Blind	75.0-84.0			25F03R5	89.03-92.53	13
25F03P5	66.5-74.0	C	20	25F03R6	75.03-88.03	21
25F03P6	59.5-65.5	C	22	25F03R7	66.53-74.03	20
25F03P7	55.0-58.5	C	23	25F03R8	59.53-65.53	22
25F03P8	51.5-54.0		6	25F03R9	55.03-58.53	23
25F03P9	3.5-50.5		5,7,24	Blind	3.53-54.03	5,6,7,24

C = Section equipped for tracer injection/sampling

Instrumentation of KI0025F02

Instrumentation was focused on Structure #19 at 132 m and ”background fracture BG#1” close to #19 at 138 m. Section P3 will be left “untouched” due to radioactive contamination from previous tracer tests.

OLD				NEW		
Borehole/section	Borehole Length		structure	Borehole/section	Borehole Length	Structure
25F02P1	135.15-204	C	25,10	25F02R1	140.05-204 C	?
25F02P2	100.25-134.15	C	19	25F02R2	135.10-139.05 C	25
25F02P3	93.40-99.25	C	13,21	25F02R3	129.2-134.10 C	19
25F02P4	78.25-92.4	C	?	25F02R4	100.25-128.2	tight
25F02P5	73.3-77.25	C	20	25F02R5	93.35-99.25 C	13,21
25F02P6	64.0-72.3	C	22	25F02R6	78.25-92.35	tight
25F02P7	56.1-63.0	C	23	25F02R7	73.3-77.25 C	20
25F02P8	51.7-55.1	C	6	25F02R8	64.0-72.3 C	22
25F02P9	38.5-50.7	C	7	25F02R9	56.1-63.0 C	23
25F02P10	3.4-37.5	C	5	25F02R10	3.4-55.1 C	5,6,7

C = Section equipped for tracer injection/sampling

Appendix 2 Distances between borehole sections, CPT-1 - CPT-4 and BS2B tests with sorbing tracers

Distances between sink section KI0025F:R2 and observation borehole sections in test CPT-1 (Andersson et al., 2004).

Borehole:sec	Secup (m)	Seclow (m)	Distance (m)
KA2511A:T1	239	293	228.0
KA2511A:T2	171	238	84.0
KA2511A:T3	139	170	101.0
KA2511A:T4	111	138	121.0
KA2511A:T5	103	110	134.0
KA2511A:T6	96	102	140.0
KA2511A:T7	65	95	156.0
KA2511A:T8	6	64	196.0
KA2563A:S1	242	246	116.0
KA2563A:S2	236	241	116.0
KA2563A:S3	206	208	120.0
KA2563A:S4	187	190	126.0
KA2563A:S5	146	186	136.0
KI0025F:R1	170.5	193.66	15.0
KI0025F:R2	165.5	169.5	**SINK**
KI0025F:R3	90.5	164.5	40.0
KI0025F:R4	87.5	89.5	79.0
KI0025F:R5	42.5	86.5	103.0
KI0025F:R6	5	41.5	144.0
KI0023B:P1	113.7	200.71	75.0
KI0023B:P2	111.25	112.7	86.0
KI0023B:P3	87.2	110.25	93.0
KI0023B:P4	84.75	86.2	101.0
KI0023B:P5	72.95	83.75	106.0
KI0023B:P6	70.95	71.95	111.0
KI0023B:P7	43.45	69.95	122.0
KI0023B:P8	41.45	42.45	134.0
KI0023B:P9	4.6	40.45	150.0

Borehole:sec	Secup (m)	Seclow (m)	Distance (m)
KI0025F02:R1	140.05	204.18	40.0
KI0025F02:R2	135.1	139.05	47.1
KI0025F02:R3	129.2	134.1	50.0
KI0025F02:R4	100.25	128.2	63.0
KI0025F02:R5	93.35	99.25	78.0
KI0025F02:R6	78.25	92.35	87.0
KI0025F02:R7	73.3	77.25	96.0
KI0025F02:R8	64	72.3	103.0
KI0025F02:R9	56.1	63	111.0
KI0025F02:R10	3.4	55.1	139.0
KI0025F03:R1	135.03	141.72	65.0
KI0025F03:R2	129.03	134.03	67.0
KI0025F03:R3	123.03	128.03	69.0
KI0025F03:R4	93.53	122.03	79.0
KI0025F03:R5	89.03	92.53	90.0
KI0025F03:R6	75.03	88.03	97.0
KI0025F03:R7	66.53	74.03	106.0
KI0025F03:R8	59.53	65.53	112.0
KI0025F03:R9	55.03	58.53	117.0
KA3510A:R1	125	150.06	181.0
KA3510A:R2	110	124	175.0
KA3510A:R3	75	109	171.0
KA3510A:R4	51	74	172.0
KA3510A:R5	4.5	50	179.0

Distances between sink section KI0025F02:R3 and observation borehole sections in test CPT-2 (Andersson et al., 2004).

Borehole:sec	Secup (m)	Seclow (m)	Distance (m)
KA2511A:T1	239	293	88.0
KA2511A:T2	171	238	65.0
KA2511A:T3	139	170	83.0
KA2511A:T4	111	138	105.0
KA2511A:T5	103	110	119.0
KA2511A:T6	96	102	126.0
KA2511A:T7	65	95	142.0
KA2511A:T8	6	64	183.0
KA2563A:S1	242	246	67.0
KA2563A:S2	236	241	66.0
KA2563A:S3	206	208	72.0
KA2563A:S4	187	190	81.0
KA2563A:S5	146	186	96.0
KI0025F:R1	170.5	193.66	63.0
KI0025F:R2	165.5	169.5	50.4
KI0025F:R3	90.5	164.5	31.2
KI0025F:R4	87.5	89.5	50.4
KI0025F:R5	42.5	86.5	71.0
KI0025F:R6	5	41.5	110.0
KI0023B:P1	113.7	200.71	42.7
KI0023B:P2	111.25	112.7	37.8
KI0023B:P3	87.2	110.25	45.7
KI0023B:P4	84.75	86.2	56.0
KI0023B:P5	72.95	83.75	62.0
KI0023B:P6	70.95	71.95	67.0
KI0023B:P7	43.45	69.95	81.0
KI0023B:P8	41.45	42.45	94.0
KI0023B:P9	4.6	40.45	112.0

Borehole:sec	Secup (m)	Seclow (m)	Distance (m)
KI0025F02:R1	140.05	204.18	40.5
KI0025F02:R2	135.1	139.05	5.4
KI0025F02:R3	129.2	134.1	**SINK**
KI0025F02:R4	100.25	128.2	17.4
KI0025F02:R5	93.35	99.25	35.4
KI0025F02:R6	78.25	92.35	46.4
KI0025F02:R7	73.3	77.25	56.0
KI0025F02:R8	64	72.3	64.0
KI0025F02:R9	56.1	63	72.0
KI0025F02:R10	3.4	55.1	102.0
KI0025F03:R1	135.03	141.72	19.4
KI0025F03:R2	129.03	134.03	18.8
KI0025F03:R3	123.03	128.03	19.5
KI0025F03:R4	93.53	122.03	29.6
KI0025F03:R5	89.03	92.53	44.1
KI0025F03:R6	75.03	88.03	52.6
KI0025F03:R7	66.53	74.03	63.0
KI0025F03:R8	59.53	65.53	71.0
KI0025F03:R9	55.03	58.53	76.0
KA3510A:P1	125	150.06	131.0
KA3510A:P2	110	124	125.0
KA3510A:P3	75	109	122.0
KA3510A:P4	51	74	125.0
KA3510A:P5	4.5	50	137.0

Distances between sink section KI0025F03:R3 and observation borehole sections in test CPT-3 (Andersson et al., 2004).

Borehole:sec	Secup (m)	Seclow (m)	Distance (m)
KA2511A:T1	239	293	90.0
KA2511A:T2	171	238	71.0
KA2511A:T3	139	170	89.0
KA2511A:T4	111	138	110.0
KA2511A:T5	103	110	125.0
KA2511A:T6	96	102	131.0
KA2511A:T7	65	95	147.0
KA2511A:T8	6	64	188.0
KA2563A:S1	242	246	49.1
KA2563A:S2	236	241	48.9
KA2563A:S3	206	208	59.0
KA2563A:S4	187	190	71.0
KA2563A:S5	146	186	89.0
KI0025F:R1	170.5	193.66	81.0
KI0025F:R2	165.5	169.5	69.0
KI0025F:R3	90.5	164.5	47.8
KI0025F:R4	87.5	89.5	54.0
KI0025F:R5	42.5	86.5	70.0
KI0025F:R6	5	41.5	105.0
KI0023B:P1	113.7	200.71	39.5
KI0023B:P2	111.25	112.7	27.0
KI0023B:P3	87.2	110.25	35.6
KI0023B:P4	84.75	86.2	46.4
KI0023B:P5	72.95	83.75	53.0
KI0023B:P6	70.95	71.95	59.0
KI0023B:P7	43.45	69.95	73.0
KI0023B:P8	41.45	42.45	87.0
KI0023B:P9	4.6	40.45	105.0
KI0025F02:R1	140.05	204.18	51.6
KI0025F02:R2	135.1	139.05	22.3
KI0025F02:R3	129.2	134.1	19.5
KI0025F02:R4	100.25	128.2	20.2
KI0025F02:R5	93.35	99.25	32.8
KI0025F02:R6	78.25	92.35	42.5
KI0025F02:R7	73.3	77.25	51.8
KI0025F02:R8	64	72.3	58.6
KI0025F02:R9	56.1	63	67.0
KI0025F02:R10	3.4	55.1	96.0
KI0025F03:R1	135.03	141.72	10.2
KI0025F03:R2	129.03	134.03	6.0
KI0025F03:R3	123.03	128.03	**SINK**
KI0025F03:R4	93.53	122.03	17.8
KI0025F03:R5	89.03	92.53	34.8
KI0025F03:R6	75.03	88.03	44.0
KI0025F03:R7	66.53	74.03	55.2
KI0025F03:R8	59.53	65.53	63.0
KI0025F03:R9	55.03	58.53	69.0

Borehole:sec	Secup (m)	Seclow (m)	Distance (m)
KA3510A:P1	125	150.06	112.0
KA3510A:P2	110	124	106.0
KA3510A:P3	75	109	105.0
KA3510A:P4	51	74	111.0
KA3510A:P5	4.5	50	126.0

Distances between injection sections and withdrawal/sink section KI0025F03:R3 used in tests CPT-4a-c and BS2B tests with sorbing tracers.

Borehole:sec	Secup (m)	Seclow (m)	Distance (m)	Test
KA2563A:S1	242	246	49.1	CPT-4b
KA2563A:S2	236	241	48.9	CPT-4b
KI0025F:R2	165.5	169.5	69.0	CPT-4a
KI0023B:P2	111.25	112.7	27.0	CPT-4a, CPT-4c
KI0025F02:R2	135.1	139.05	22.3	CPT-4b, CPT-4c, BS2B sorbing
KI0025F02:R3	129.2	134.1	19.5	CPT-4a, CPT-4c, BS2B sorbing
KI0025F03:R3	123.03	128.03	**SINK**	CPT-4a-c, BS2B sorbing